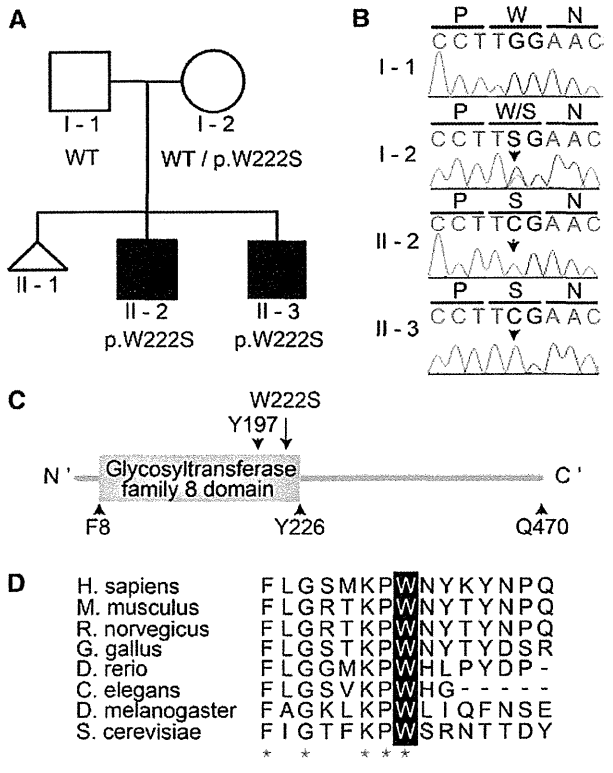

Fig. 1 Mutation Analysis of *GYG2*. **a** Pedigree of the family with a unique type of LS and a *GYG2* mutation (c.665G>C, p.W222S). *Square*, *circle* and *triangle* denote male, female and spontaneous abortion, respectively. *White* and *black symbols* indicate unaffected and affected individuals, respectively, while the affection status of the spontaneous abortion is unknown. **b** Electropherograms of a *GYG2* mutation. **c** The functional domain of human GYG2 (isoform a). The substitution of p.W222S is located within the glycosyltransferase family 8 domain (*yellow square*). **d** The evolutionary conservation of the W222 in GYG2. *Red stars* indicate identical amino acids from *S. cerevisiae* to *H. sapiens*. Sequences were aligned using CLUSTALW (http://www.genome.jp/tools/clustalw/)

missense mutation (c.665G>C, p.W222S) was introduced by Site-directed mutagenesis using the QuikChange II XL site-directed mutagenesis kit (Agilent Technologies, Santa Clara, CA). Wild-type and mutant C' V5/6xHis tagged GYG2 constructs were created using pcDNA-DEST40 (Invitrogen, Carlsbad, CA) by LR recombination in Gateway system (Invitrogen). To create the untagged construct, the last codon was altered to a stop codon by mutagenesis.

Self-glucosylation analysis

Glucosyltransferase activity of GYG2 was measured as previously described (Lomako et al. 1988), with slight modifications. In brief, COS-1 cells were maintained in Dulbecco's modified Eagle's medium (DMEM) (Sigma-Aldrich, Schnelldorf, Germany) containing 10 % heat-inactivated fetal bovine serum (FBS) (Gibco-BRL, Grand Island, NY), 2 mM L-glutamine (Sigma-Aldrich) and 1 % penicillin–streptomycin (Sigma-Aldrich). As previously described (Mu and Roach 1998), the ~80 % confluent COS-1 cells (~1 × 10^7) were transiently transfected by X-treamGENE9 DNA transfection reagent (Roche Applied Science, Foster City, CA) with 5 μg of either a wild-type Human GYG2 (isoform a) expressing plasmid or the same plasmid into which the W222S encoding mutation had been introduced. After 24 h, the cells were collected and lysed in 300 μl of buffer consisting of 50 mM HEPES, 0.5 % Triton X-100, 1 × EDTA-free protease Inhibitor Cocktail tablets (Roche Applied Science), 1 × phosphatase inhibitor cocktail (Nacalai Tesque Inc., Kyoto, Japan) and 0.5 mM β-mercaptoethanol (Mu et al. 1997). After centrifugation at 14,000 rpm for 15 min, 10 μl of the soluble fractions were mixed with 10 μl of 2 × reaction buffer containing 100 mM HEPES (pH7.5), 10 mM MgCl, 4 mM dithiothreitol (DTT) and 40 μM UDP-[^{14}C]-glucose (250 mCi/mmol; PerkinElmer, Waltham, MA) (Cao et al. 1993). After incubation at 30 °C for 30 min, the reaction was stopped by addition of 20 μl of 2 × Laemmli sample buffer (Sigma-Aldrich) (Viskupic et al. 1992). 15 μl of each sample was subjected to SDS-polyacrylamide gel electrophoresis. After treatment with Gel drying solution (Bio-Rad Laboratories, Hercules, CA) for 30 min, gels were dried. Dried gels were then exposed on X-ray film for 2 weeks to detect the incorporation of UDP-[^{14}C]-glucose into GYG2. In addition, the ^{14}C-signal intensities were evaluated using an imaging analyzer, BAS2500 (Fujifilm). Three independent experiments were performed.

Western blot analysis

For the detection of GYG2 protein, rabbit polyclonal anti-GYG2 antibodies (1:500 dilution; Abcam Inc., Cat.#HPA005495, Cambridge, MA) and horse-radish peroxidase (HRP)-conjugated anti-rabbit IgG (1:10,000 dilution; Jackson ImmunoResearch, Cat.#111-035-003, West Grove, PA) were used. Immunoblot chemiluminescence was performed using SuperSignal West Dura as substrate (Thermo Fisher Scientific, Waltham, MA). The chemiluminescence signal images were captured by FluorChem 8900 (Alpha Innotech, San Leandro, CA). Signal intensities were measured by AlphaEase FC (Alpha Innotech). Three independent experiments were performed.

Results

Clinical finding

Patient II-2 (Fig. 1a; Table 1) is a 26-year-old male born to non-consanguineous parents. His mother previously had a

Table 1 Clinical features of the presenting patients affected with LS

	II-2	II-3
Sex	M	M
Age (years)	26	19
Common clinical phenotype		
Psychomotor retardation	+	+
Failure to thrive	+	+
Swallowing difficulties	−	−
Spasticity	+	+
Rigidity	+	+
Pathological reflexes	+	+
Ataxia	+	+
Athetoid movements	+	+
Convulsions	+	+
Ophthalmoplegia	+	+
Strabismus	+	+
Gastrointestinal problems	+	+
Renal agenesis	NA	+
Pes equinovarus	+	+
Uncommon clinical phenotype		
Increase of ketone body	+	+

NA not assessed

spontaneous abortion. He was born at 39 weeks gestation without asphyxia after an uneventful pregnancy. His body weight was 3,680 g (+1.6 SD), his height was 50.0 cm (−0.5 SD), and his head circumference (HC) was 34.0 cm (−0.5 SD). His early developmental milestones were normal with head control and reach to toys at 4 months, roll at 6 months and grasp with two fingers at 7 months. At 10 months, he was referred to our hospital because of an inability to sit. His body weight was 9,120 g (±0.0 SD), his height was 76.0 cm (+1.3 SD), and his HC was 48.0 cm (+1.4 SD). He could smile and swallow well. Bilateral strabismus was noted. No minor anomalies were noticed. Muscle tone was normal. Deep tendon reflexes were normal with negative Babinski sign. He showed athetoid movements of trunk and extremities. He showed pes equinovarus at traction response. Levels of lactate and pyruvate were normal with 12.2 and 0.89 mg/dl (L/P ratio = 13.7), respectively. Other laboratory examinations, including blood gas, blood sugar, ammonia, AST, ALT, BUN, Creatine, TSH, T3, T4, amino acids, and urine organic acid analyses were all normal. Electroencephalogram (EEG) showed no abnormalities. He was suspected to have dyskinetic cerebral palsy and referred to the division of rehabilitation. He could crawl at the age of 2. At 6 years, he experienced a loss of consciousness followed by generalized tonic–clonic convulsion with fever and was admitted to another hospital. He was diagnosed with bilateral infarction of the basal ganglia. Although EEG showed no abnormalities, clonazepam was started with the suspicion of symptomatic epilepsy. At the age of 9, he was referred to us again. His weight was 19.1 kg (−4.5 SD), his height was 115.0 cm (−2.8 SD). He lost the ability to speak several words and switched handedness from right to left. He also showed other signs of regression: including spasticity with elevated deep tendon reflexes and positive Babinski sign. In addition, he suffered bilateral hip joint dislocations and the foot deformity became worse. Contractures were noted in all extremities. Brain magnetic resonance imaging (MRI) revealed a bilateral necrotic lesion of the globus pallidus (Fig. 2a, b). EEG and motor conduction velocities were normal. Laboratory examinations, including lactate and pyruvate, were all normal. At the age of 12, he was admitted with acute bronchitis, at that time he showed an increase of blood ketone bodies: acetoacetic acid, 720 μmol/l; 3OHBA, 974 μmol/l and urine ketone (+++). Blood levels of ammonia (18 μmol/l), sugar (125 mg/dl) and lactate/pyruvate (5.1/0.29 mg/dl) were all within normal range. The values of blood ketone bodies returned to normal level with the cease of fever. Deficiencies of 3-ketothiolase and succinyl-CoA:3-oxoacid CoA transferase were ruled out by enzyme analysis using fibroblasts. His clinical symptoms and repeated MRI show the non-progressive course of his disease. Currently he is unable to sit or speak any words. Despite the addition of carbamazepine and lamotrigine, he still exhibits generalized tonic–clonic convulsion a few times a year. He also takes medicine for hypertonicity including dantrolene sodium, diazepam, baclofen and levodopa.

Patient II-3 (Fig. 1a; Table 1), the younger brother of II-2, was born uneventfully. He was born at 37 week's gestation without asphyxia after an uneventful pregnancy. His body weight was 3,668 g (+1.5 SD), his height was 50.0 cm (+0.5 SD), and his HC was 36.0 cm (−0.5 SD). He suffered from bacterial meningitis of unknown origin at 1 month of age. He became unconscious followed by convulsion and gastroenteritis at 1 year and 11 months. Brain MRI showed marked swelling of the basal ganglia (Fig. 2c, d). He was diagnosed with bilateral infarction of the basal ganglia. After this event, he became left handed. When he was 2 years old, surgery was performed to correct bilateral inner strabismus. He was referred to our hospital at the age of 4 for evaluation. His body weight was 11.0 kg (−2.2 SD), his height was 92.5 cm (−1.2 SD), and his HC was 49.5 cm (−1.3 SD). He could respond with a smile to his mother's voice. Motor milestones were delayed with no head control. No minor anomalies were noticed. Muscle tone was hypotonic. Deep tendon reflexes were exaggerated with positive Babinski sign and ankle clonus. He showed pes equinovarus. He showed a significant increase of blood acetoacetic acid of 1,270 μmol/l and 3-OHBA of 3,270 μmol/l. Levels of blood lactate and pyruvate were normal (6.2 and 0.48 mg/dl, respectively, L/P ratio = 12.9).

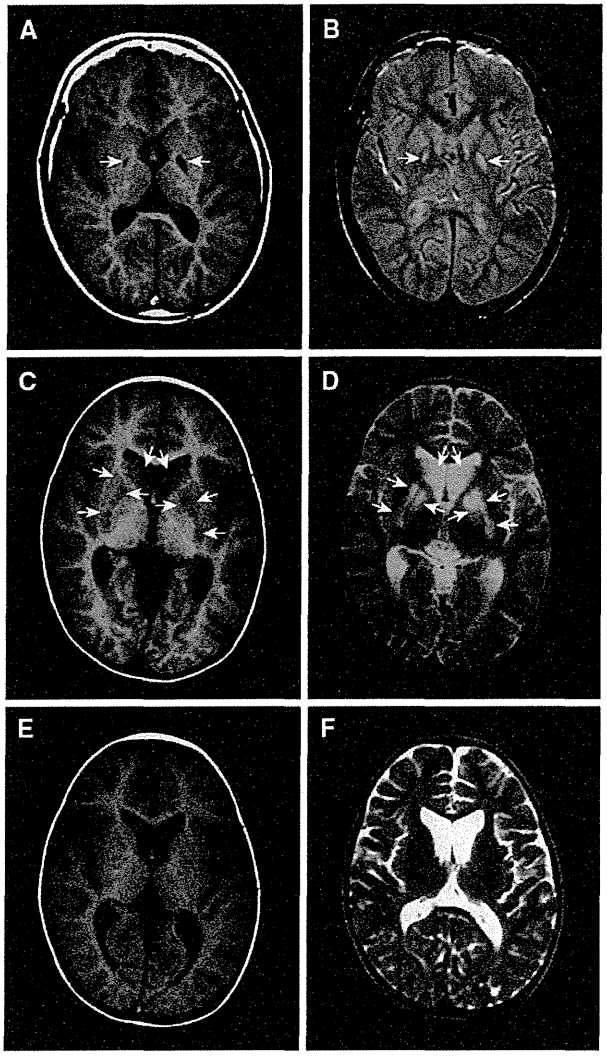

Fig. 2 Brain MRI of affected patients with a *GYG2* mutation. **a**, **b** (Patient II-2): T1 (**a**) and T2 (**b**) weighted brain magnetic resonance imaging (MRI) show necrotic lesion of bilateral globus pallidus (*arrows*). T2 elongation is observed at deep white matter at 1 year. **c–f** (Patient II-3): MRI at 1 year and 11 months shows swellings of caudate nuclei, globus pallidus, and putamen with the decreased T1 intensity (**c**) and increased T2 signals (**d**). *Arrows* indicate swollen lesions in basal ganglia. At 4 years (**e**, **f**), swelling of basal ganglia disappeared with continued mild high intensity in T2 weighted image (**f**)

Lactate and pyruvate levels of cerebrospinal fluid were slightly elevated with 11.3 and 1.11 mg/dl, respectively. Other laboratory examinations, including blood gas, blood sugar, ammonia, AST, ALT, BUN, Creatine, TSH, T3, T4, amino acids, and lysosomal enzymes were all normal. Urine organic acid analyses showed an increase of acetoacetic acid, 3-OHBA, and 3-OH-isovaleric acid. EEG showed no paroxysmal discharges. Muscle biopsy showed no specific abnormalities and no ragged red fibers. Staining for cytochrome c oxidase was normal (data not shown). Brain MRI disclosed T2 elongation in the basal ganglia and cerebral deep white matter (Fig. 2e, f). At the age of 5, he showed lethargy with fever. At 6 years, he again showed lethargy. Biochemical analysis disclosed a significant increase of blood ketone bodies: acetoacetic acid, 1,337 μmol/l; 3-OHBA, 4,845 μmol/l and urine ketone (+++). Blood levels of ammonia (28 μmol/l), sugar (78 mg/dl), lactate (5.1 mg/dl) and pyruvate (0.43 mg/dl) were all within normal range. Blood gas analysis revealed metabolic ketoacidosis with an increase of anion gap; 22.4 mEq/l (normal range 12 ± 2). His consciousness and biochemical measurements returned to normal within a few days with intravenous fluid infusion. Similar ketoacidosis attacks were repeatedly observed and agenesis of the left kidney and neurogenic bladder were recognized at the age of 8. He started intermittent urinary catheterization, and suffered from repeated urinary tract infections, resulted in chronic renal failure. Repeated brain MRI shows the progression of cerebral and cerebellar atrophy. He is now 19 years old and shows no gain of motor or intellectual abilities from the age of 4. He takes dantrolene sodium and diazepam for hypertonicity, and spherical charcoal, allopurinol for renal failure.

Identification of a *GYG2* variant by exome sequencing

A total of 2,433,011,483 bps (II-2) and 7,926,169,749 bps (II-3) were mapped to RefSeq coding DNA sequence (CDS). 83.3 and 96.0 % of CDS were covered by ten reads and more. We used only NGS data of II-3 for selecting candidate variants as the lower-quality NGS data of II-2 may lead to erroneous conclusion. Based on the hypothesis that this syndrome is inherited in an autosomal recessive or an X-linked recessive fashion, we focused on homozygous or compound heterozygous variants on autosomes and hemizygous variants on the X chromosome. While nine variants in four candidate genes were selected by in silico flow, only one hemizygous missense mutation in *GYG2* gene agreed with the familial segregation pattern (autosomal recessive or X-linked recessive) (Table S1, S2). The c.665G>C (p.W222S) in *GYG2* (isoform a: NM_001079855) was hemizygous in affected sibs and heterozygous in their mother, consistent with the X-linked recessive model, and was confirmed by Sanger sequence (Fig. 1b). The variant was absent in our in-house Japanese exome data ($n = 418$), the 1,000 Genomes database and ESP6500. Furthermore, no pathological variants in mtDNA were detected by exome sequence (Supplementary Results, Figure S1). In addition, a total of 21 LS patients (12 males and 9 females) were screened, but no pathological changes were found in *GYG2*.

GYG2 encodes GYG2 proteins with at least five isoforms: isoform a (NM_001079855), isoform b (NM_003918),

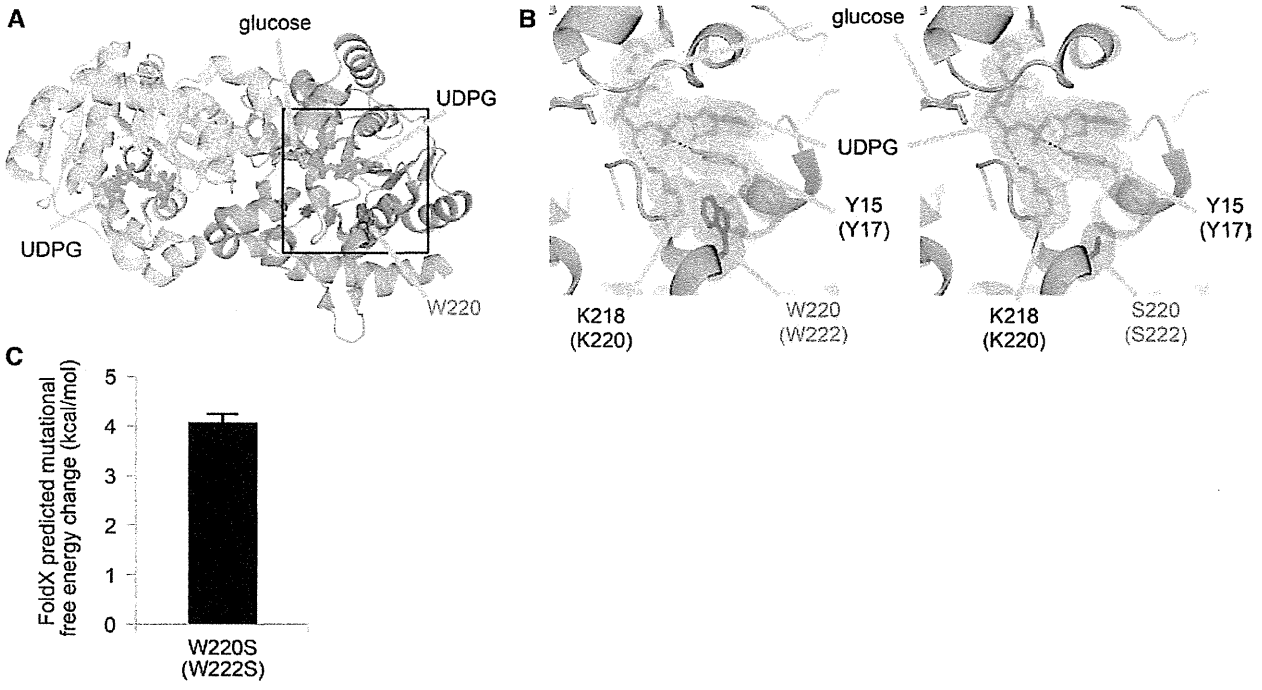

Fig. 3 Molecular structural consideration of the W222S mutation of GYG2. **a** Crystal structure of human GYG1 (Protein Data Bank code; 3T7O) (Chaikuad et al. 2011). Each monomer is colored *yellow* and *cyan*. α-helices, β-sheet and loops are drawn as *ribbons*, *arrows* and *threads*, respectively. The side chain of W222, glucose and UDP-glucose (UDPG) are shown as *sticks* in *red*, *orange* and *green*, respectively. Amino acid numbering shown is for human GYG1 with that for human GYG2 in *parenthesis*. The *squared area* corresponds to the close-up views in (**b**). **b** Detailed views of structures of the wild-type (*left*) and mutated GYG2 (p.W222S) (*right*). Amino acid residues at positions of 15, 218 and 220 and UDPG are shown as sticks with van der Waals representation and annotations. Hydrogen bonds are depicted as *dotted lines*. **c** Calculated free energy change upon the p.W222S mutation of GYG2 using FoldX software. All the molecular structures were drawn using PyMOL (www.pymol.org)

isoform c (NM_001184702), isoform d (NM_001184703), and isoform e (NM_001184704). At least two GYG2 isoforms (isoform a and b) are expressed preferentially in liver, heart and pancreas (Mu et al. 1997), while the detailed expression and function of other isoforms are undetermined. GYG2 has a glycosyltransferase family 8 domain and initiates glucose addition on its Tyrosine residue (Y197 in isoform a) via *O*-glycosylation (self-glucosylation) and can also attach an additional 7–10 residues of UDP-glucose to itself (Bollen et al. 1998; Lomako et al. 2004; Zhai et al. 2001). The W222 within the glycosyltransferase family 8 domain is evolutionarily highly conserved from *S. cerevisiae* to *H. sapiens* (Fig. 1c, d). In addition, all isoforms contain this residue. Thus, it is thought that this mutation may impair its biological function.

Structural consideration of the p.W222S mutation in human GYG2

The amino acid residue W222 of GYG2 (isoform a) was mapped to the crystal structure of human GYG1 (Chaikuad et al. 2011), since no experimental structure of GYG2 was available. W222 is involved in a hydrophobic core near the UDP-glucose (UDPG) binding site along with Y17 and K220 (Fig. 3a, b). The side chains of Y17 and K220 are hydrogen-bonded to UDPG, and the former also makes van der Waals contacts with the uridine ring of UDPG in a stacking mode. Therefore, the formation of the hydrophobic core appears to be a prerequisite for UDPG binding. To estimate the impact of the W222S mutation on the protein stability, we modeled the mutant structure and calculated the free energy change upon the mutation using the FoldX software. As a result, the mutation was predicted to destabilize the protein structure with about 4 kcal/mol increase in free energy (Fig. 3c). This suggests that the W222S mutation would impair UDPG binding (Fig. 3b).

Self-glucosylation analysis

To see the functional effects of the *GYG2* mutation in vitro, glucosyltransferase activity monitoring by self-glucosylation was measured using wild-type (WT) and W222S mutant (Mut) GYG2 (isoform a) transiently

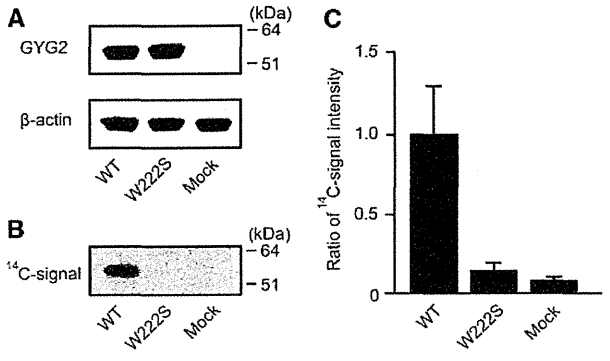

Fig. 4 Enzyme activity of GYG2. **a** Western blot analysis of recombinant GYG2. Wild-type (WT) and mutant (p.W222S) GYG2 was detected at the expected size (52 kDa). β-actin (42 kDa) was used as an internal control. **b** Autoradiography images presenting ^{14}C glucosylation toward GYG2. The signal was detected in WT, but undetected in mutant, with similar levels to Mock. **c** Graphic presentation of autoglucosylation of GYG2. The activity detected in Mock might be due to the endogenous glycogenin. *Error bars* represent the standard error of the mean

overexpressed in COS-1 cells. By immunoblotting, the expected 52 kDa bands of recombinant WT and Mut GYG2 were detected with similar expression levels (Fig. 4a). While WT GYG2 showed reasonable glucosyltransferase activity, Mut GYG2 almost completely lost the enzyme activity and was similar to the Mock level (Fig. 4b, c).

Expression analysis of GYG1 and GYG2

To observe tissue distribution of the human *GYG1* and *GYG2*, expression analysis was performed using multiple tissue cDNA panels. *GYG1* was expressed preferentially in skeletal muscle and heart from fetus to adult stages as previous reports (Barbetti et al. 1996). *GYG2* is dominantly expressed in liver from fetus through adult stages and moderately expressed in brain, heart, pancreas and kidney (Supplementary Results, Figure S2). To be marked, *GYG1* is not expressed in liver and brain where *GYG2* is highly expressed.

Discussion

In this study, we analyzed unique brothers affected with LS who were born to non-consanguineous healthy parents after uneventful pregnancies. Patient II-2 and II-3 developed LS accompanied by delayed developmental milestones at 10 months and 13 months of age, respectively. Their age of onset, clinical features and brain imaging were compatible with the diagnosis of LS. Interestingly, CNS abnormalities were observed (developmental delay, convulsion, athetoid movements, nystagmus, hypotonia, spasticity, increased deep tendon reflex and abnormal reflection), but involvement of peripheral nerve and extraneural organs was obscure. Based on the facts including (1) male (X-linked recessive), (2) normal lactate/pyruvate, (3) ketonemia/ketonuria, and (4) CNS predominant symptoms, the hemizygous *GYG2* mutation was highlighted a primary culprit.

In this study, we first identified a human *GYG2* mutation in affected brothers with LS with ketonemia/ketonuria but normal blood lactate/pyruvate. We can hypothesize a pathomechanism of the *GYG2* impairment in this family based on the canonical pathway of glycogen metabolism (Fig. 5). As glycogen storage in liver might be decreased because of the GYG2 malfunction, glucose is easily depleted. To keep appropriate blood glucose concentrations, the metabolism would be shifted toward gluconeogenesis and beta-oxidation to create glucose and energy sources like Acetyl-CoA (Garber et al. 1974; Laffel 1999; Randle et al. 1964). Excess beta-oxidation would result in overproduction of ketone bodies, consistent with the observation of ketonemia and ketonuria. However, pyruvate and lactate could be normally metabolized in gluconeogenesis and/or TCA cycle and would not accumulate in the body as seen in the majority of LS patients. Interestingly, both patients showed normal blood glucose level while showing LS manifestations which might be due to tissue energy depletion. In GYG2-deficient patients, the CNS was dominantly affected, while the effect of this abnormal metabolism was thought to extend to the entire body. This predominance could be explained by high glucose consumption as the primary energy source in brain (Amaral 2012; Magistretti and Pellerin 1999) and glycogen depletion in brain tissue level, while the blood sugar level was maintained by the other compensatory mechanism. This is similar to the muscle specific phenotypes (muscle weakness and arrhythmia) observed in patients with deficiencies of "muscle form" GYG1 in the absence of hypoglycemia (Moslemi et al. 2010). Remarkably, glycogen was less in the muscle tissue of GYG1 depleted patient (Moslemi et al. 2010). These evidences might indicate that it is not always linked between glucose level in the peripheral blood and glycogen/energy supply in tissue level while we could not show the loss of glycogen in liver or brain tissues because the materials were not available. In addition, deficiencies in two paralogous enzymes, GYG1 and GYG2, result in different human diseases suggesting they are unable to compensate each other in specific organs.

The *GYG2* mutation is probably causative for LS in this family. However, it is possible that the mutation is just coincidence because we just showed genetic evidences (due

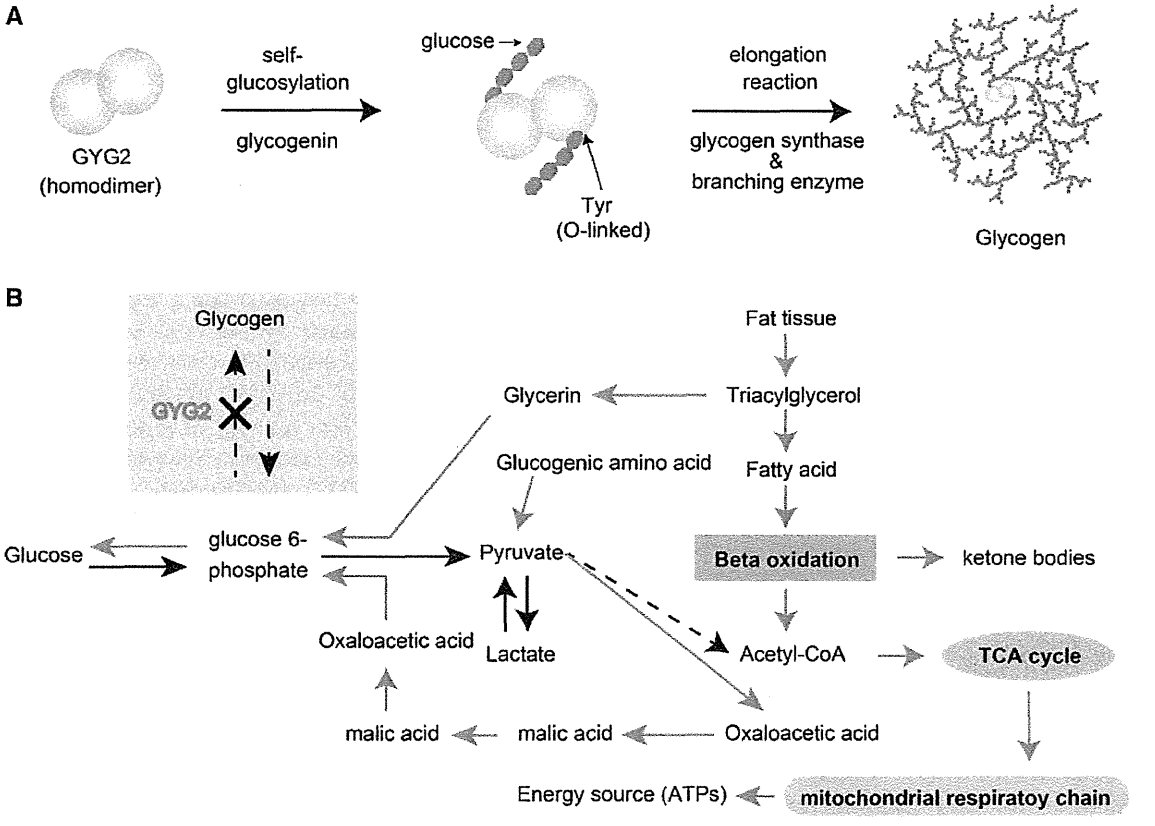

Fig. 5 Biochemical metabolisms in glycogen storage and glycolysis pathways. **a** Schematic presentation of glycogen biosynthesis. GYG2 has a catalytic capability for *O*-linked self-glucosylation at Tyrosine (Y197 in isoform a) and adds approximately 10 glucose molecules. By the subsequent elongating reactions by glycogen synthase and branching enzyme, giant molecule "glycogen" is formed. **b** Modeled biochemical pathway in GYG2 impairment. As the GYG2 impairment results in the absence of glycogen storage, glycogen is easy to be depleted and gluconeogenesis is induced from fat tissues and glucogenic amino acids. The reactions in mitochondria are shown in *yellow shadow*. While increased acetyl-CoA inhibits the pyruvate dehydrogenase complex which irreversibly converts pyruvate to acetyl-CoA (as shown as *dotted line*), it accelerates gluconeogenesis through pyruvate–oxaloacetic acid–malic acid–oxaloacetic acid. Triacylglycerol was metabolized into glycerin and fatty acid. Fatty acid was used for beta-oxidation and ketone production. The *arrows* indicate the directions of normal metabolism. *Red arrows* indicate the predicted predominant pathways in GYG2-deficient patients

to its rarity and familial co-segregation) and GYG2 loss of function by in vitro study without showing any sufficient data on how the *GYG2* mutation causes LS.

In conclusion, we describe the first human variant of *GYG2* which may be associated with the atypical LS phenotype in this family. Further studies are absolutely needed to conclude whether *GYG2* abnormality leads to atypical LS observed in this family.

Acknowledgments We thank all the patients and their families for participating in this work. We deeply appreciate Dr. Toshiyuki Fukao, who is the professor of Department of Pediatrics, Graduate School of Medicine, Gifu University, for the enzyme assay for 3-ketothiolase deficiency and succinyl-CoA:3-oxoacid CoA transferase. We would like to thank Dr. Yasushi Okazaki at Research Center for Genomic Medicine, Saitama Medical University for helpful discussion. We also thank Ms. Y. Yamashita, S. Sugimoto and K. Takabe for their technical assistance. This work was supported by research grants from the Ministry of Health, Labour, and Welfare (H. Saitsu, N. Matsumoto and N. Miyake), the Japan Science and Technology Agency (N. Matsumoto), the Strategic Research Program for Brain Sciences (to N. Matsumoto), a Grant-in-Aid for Scientific Research on Innovative Areas (Transcription Cycle) from the Ministry of Education, Culture, Sports, Science, and Technology of Japan (N. Matsumoto), a Grant-in-Aid for Scientific Research from the Japan Society for the Promotion of Science (to N. Matsumoto), a Grant-in-Aid for Young Scientists from the Japan Society for the Promotion of Science (H. Saitsu and N. Miyake), a grant from the 2012 Strategic Research Promotion of Yokohama City University (N. Matsumoto), and research grants from the Japan Epilepsy Research Foundation (H. Saitsu) and the Takeda Science Foundation (N. Matsumoto and N. Miyake).

Conflict of interest The authors declare that they have no conflict of interest.

References

Amaral AI (2012) Effects of hypoglycaemia on neuronal metabolism in the adult brain: role of alternative substrates to glucose. J Inherit Metab Dis. doi:10.1007/s10545-012-9553-3

Antonicka H, Ostergaard E, Sasarman F, Weraarpachai W, Wibrand F, Pedersen AM, Rodenburg RJ, van der Knaap MS, Smeitink JA, Chrzanowska-Lightowlers ZM, Shoubridge EA (2010) Mutations in C12orf65 in patients with encephalomyopathy and a mitochondrial translation defect. Am J Hum Genet 87:115–122. doi:10.1016/j.ajhg.2010.06.004

Barbetti F, Rocchi M, Bossolasco M, Cordera R, Sbraccia P, Finelli P, Consalez GG (1996) The human skeletal muscle glycogenin gene: cDNA, tissue expression and chromosomal localization. Biochem Biophys Res Commun 220:72–77. doi:10.1006/bbrc.1996.0359

Benke PJ, Parker JC Jr, Lubs ML, Benkendorf J, Feuer AE (1982) X-linked Leigh's syndrome. Hum Genet 62:52–59

Bollen M, Keppens S, Stalmans W (1998) Specific features of glycogen metabolism in the liver. Biochem J 336:19–31

Brown GK, Squier MV (1996) Neuropathology and pathogenesis of mitochondrial diseases. J Inherit Metab Dis 19:553–572

Cao Y, Mahrenholz AM, DePaoli-Roach AA, Roach PJ (1993) Characterization of rabbit skeletal muscle glycogenin. Tyrosine 194 is essential for function. J Biol Chem 268:14687–14693

Chaikuad A, Froese DS, Berridge G, von Delft F, Oppermann U, Yue WW (2011) Conformational plasticity of glycogenin and its maltosaccharide substrate during glycogen biogenesis. Proc Natl Acad Sci USA 108:21028–21033. doi:10.1073/pnas.1113921108

Debray FG, Morin C, Janvier A, Villeneuve J, Maranda B, Laframboise R, Lacroix J, Decarie JC, Robitaille Y, Lambert M, Robinson BH, Mitchell GA (2011) LRPPRC mutations cause a phenotypically distinct form of Leigh syndrome with cytochrome c oxidase deficiency. J Med Genet 48:183–189. doi:10.1136/jmg.2010.081976

Farina L, Chiapparini L, Uziel G, Bugiani M, Zeviani M, Savoiardo M (2002) MR findings in Leigh syndrome with COX deficiency and SURF-1 mutations. AJNR Am J Neuroradiol 23:1095–1100

Finsterer J (2008) Leigh and Leigh-like syndrome in children and adults. Pediatr Neurol 39:223–235. doi:10.1016/j.pediatrneurol.2008.07.013

Garber AJ, Menzel PH, Boden G, Owen OE (1974) Hepatic ketogenesis and gluconeogenesis in humans. J Clin Invest 54:981–989. doi:10.1172/JCI107839

Gibbons BJ, Roach PJ, Hurley TD (2002) Crystal structure of the autocatalytic initiator of glycogen biosynthesis, glycogenin. J Mol Biol 319:463–477. doi:10.1016/S0022-2836(02)00305-4

Guerois R, Nielsen JE, Serrano L (2002) Predicting changes in the stability of proteins and protein complexes: a study of more than 1000 mutations. J Mol Biol 320:369–387. doi:10.1016/S0022-2836(02)00442-4

Khan S, Vihinen M (2010) Performance of protein stability predictors. Hum Mutat 31:675–684. doi:10.1002/humu.21242

Krisman CR, Barengo R (1975) A precursor of glycogen biosynthesis: alpha-1,4-glucan-protein. Eur J Biochem 52:117–123

Laffel L (1999) Ketone bodies: a review of physiology, pathophysiology and application of monitoring to diabetes. Diabetes Metab Res Rev 15:412–426

Larner J (1953) The action of branching enzymes on outer chains of glycogen. J Biol Chem 202:491–503

Leigh D (1951) Subacute necrotizing encephalomyelopathy in an infant. J Neurol Neurosurg Psychiatry 14:216–221

Lomako J, Lomako WM, Whelan WJ (1988) A self-glucosylating protein is the primer for rabbit muscle glycogen biosynthesis. FASEB J 2:3097–3103

Lomako J, Lomako WM, Whelan WJ (2004) Glycogenin: the primer for mammalian and yeast glycogen synthesis. Biochim Biophys Acta 1673:45–55. doi:10.1016/j.bbagen.2004.03.017

Lopez LC, Schuelke M, Quinzii CM, Kanki T, Rodenburg RJ, Naini A, Dimauro S, Hirano M (2006) Leigh syndrome with nephropathy and CoQ10 deficiency due to decaprenyl diphosphate synthase subunit 2 (PDSS2) mutations. Am J Hum Genet 79:1125–1129. doi:10.1086/510023

Magistretti PJ, Pellerin L (1999) Cellular mechanisms of brain energy metabolism and their relevance to functional brain imaging. Philos Trans R Soc Lond B Biol Sci 354:1155–1163. doi:10.1098/rstb.1999.0471

Martin MA, Blazquez A, Gutierrez-Solana LG, Fernandez-Moreira D, Briones P, Andreu AL, Garesse R, Campos Y, Arenas J (2005) Leigh syndrome associated with mitochondrial complex I deficiency due to a novel mutation in the NDUFS1 gene. Arch Neurol 62:659–661. doi:10.1001/archneur.62.4.659

Medina L, Chi TL, DeVivo DC, Hilal SK (1990) MR findings in patients with subacute necrotizing encephalomyelopathy (Leigh syndrome): correlation with biochemical defect. AJR Am J Roentgenol 154:1269–1274

Moslemi AR, Lindberg C, Nilsson J, Tajsharghi H, Andersson B, Oldfors A (2010) Glycogenin-1 deficiency and inactivated priming of glycogen synthesis. N Engl J Med 362:1203–1210. doi:10.1056/NEJMoa0900661

Mu J, Roach PJ (1998) Characterization of human glycogenin-2, a self-glucosylating initiator of liver glycogen metabolism. J Biol Chem 273:34850–34856

Mu J, Skurat AV, Roach PJ (1997) Glycogenin-2, a novel self-glucosylating protein involved in liver glycogen biosynthesis. J Biol Chem 272:27589–27597

Naess K, Freyer C, Bruhn H, Wibom R, Malm G, Nennesmo I, von Dobeln U, Larsson NG (2009) MtDNA mutations are a common cause of severe disease phenotypes in children with Leigh syndrome. Biochim Biophys Acta 1787:484–490. doi:10.1016/j.bbabio.2008.11.014

Ostergaard E, Hansen FJ, Sorensen N, Duno M, Vissing J, Larsen PL, Faeroe O, Thorgrimsson S, Wibrand F, Christensen E, Schwartz M (2007) Mitochondrial encephalomyopathy with elevated methylmalonic acid is caused by SUCLA2 mutations. Brain 130:853–861. doi:10.1093/brain/awl383

Picardi E, Pesole G (2012) Mitochondrial genomes gleaned from human whole-exome sequencing. Nat Methods 9:523–524. doi:10.1038/nmeth.2029

Pitcher J, Smythe C, Cohen P (1988) Glycogenin is the priming glucosyltransferase required for the initiation of glycogen biogenesis in rabbit skeletal muscle. Eur J Biochem 176:391–395

Quinonez SC, Leber SM, Martin DM, Thoene JG, Bedoyan JK (2013) Leigh syndrome in a girl with a novel DLD mutation causing E3 deficiency. Pediatr Neurol 48:67–72. doi:10.1016/j.pediatrneurol.2012.09.013

Rahman S, Blok RB, Dahl HH, Danks DM, Kirby DM, Chow CW, Christodoulou J, Thorburn DR (1996) Leigh syndrome: clinical features and biochemical and DNA abnormalities. Ann Neurol 39:343–351. doi:10.1002/ana.410390311

Randle PJ, Newsholme EA, Garland PB (1964) Regulation of glucose uptake by muscle. 8. Effects of fatty acids, ketone bodies and pyruvate, and of alloxan-diabetes and starvation, on the uptake and metabolic fate of glucose in rat heart and diaphragm muscles. Biochem J 93:652–665

Smythe C, Caudwell FB, Ferguson M, Cohen P (1988) Isolation and structural analysis of a peptide containing the novel tyrosyl-glucose linkage in glycogenin. EMBO J 7:2681–2686

van Erven PM, Cillessen JP, Eekhoff EM, Gabreels FJ, Doesburg WH, Lemmens WA, Slooff JL, Renier WO, Ruitenbeek W (1987)

Leigh syndrome, a mitochondrial encephalo(myo)pathy. A review of the literature. Clin Neurol Neurosurg 89:217–230

Viskupic E, Cao Y, Zhang W, Cheng C, DePaoli-Roach AA, Roach PJ (1992) Rabbit skeletal muscle glycogenin. Molecular cloning and production of fully functional protein in Escherichia coli. J Biol Chem 267:25759–25763

Zhai L, Schroeder J, Skurat AV, Roach PJ (2001) Do rodents have a gene encoding glycogenin-2, the liver isoform of the self-glucosylating initiator of glycogen synthesis? IUBMB Life 51:87–91. doi:10.1080/15216540117315

Neurogenetics (2013) 14:225–232
DOI 10.1007/s10048-013-0375-8

ORIGINAL ARTICLE

Diagnostic utility of whole exome sequencing in patients showing cerebellar and/or vermis atrophy in childhood

Chihiro Ohba · Hitoshi Osaka · Mizue Iai · Sumimasa Yamashita · Yume Suzuki · Noriko Aida · Nobuyuki Shimozawa · Ayumi Takamura · Hiroshi Doi · Atsuko Tomita-Katsumoto · Kiyomi Nishiyama · Yoshinori Tsurusaki · Mitsuko Nakashima · Noriko Miyake · Yoshikatsu Eto · Fumiaki Tanaka · Naomichi Matsumoto · Hirotomo Saitsu

Received: 9 July 2013 / Accepted: 18 September 2013 / Published online: 4 October 2013

Abstract Cerebellar and/or vermis atrophy is recognized in various types of childhood disorders with clinical and genetic heterogeneity. Although careful evaluation of clinical features and neuroimaging can lead to correct diagnosis of disorders, their diagnosis is sometimes difficult because clinical features can overlap with each other. In this study, we performed family-based whole exome sequencing of 23 families including 25 patients with cerebellar and/or vermis atrophy in childhood, who were unable to be diagnosed solely by clinical examination. Pathological mutations of seven genes were found in ten patients from nine families (9/23, 39.1 %): compound heterozygous mutations in *FOLR1*, *C5orf42*, *POLG*, *TPP1*, *PEX16*, and de novo mutations in *CACNA1A*, and *ITPR1*. Patient 1A with *FOLR1* mutations showed extremely low concentration of 5-methyltetrahydrofolate in the cerebrospinal fluid and serum, and Patient 6 with *TPP1* mutations demonstrated markedly lowered tripeptidyl peptidase 1 activity in leukocytes. Furthermore, Patient 8 with *PEX16* mutations presented a mild increase of very long chain fatty acids in the serum as supportive data for genetic diagnosis. The main clinical features of these ten patients were nonspecific and mixed, and included developmental delay, intellectual disability, ataxia, hypotonia, and epilepsy. Brain MRI revealed both cerebellar and vermis atrophy in eight patients (8/10, 80 %), vermis atrophy/hypoplasia in two patients (2/10, 20 %), and brainstem atrophy in one patient (1/10, 10 %).

Electronic supplementary material The online version of this article (doi:10.1007/s10048-013-0375-8) contains supplementary material, which is available to authorized users.

C. Ohba · K. Nishiyama · Y. Tsurusaki · M. Nakashima · N. Miyake · N. Matsumoto (✉) · H. Saitsu (✉)
Department of Human Genetics, Graduate School of Medicine, Yokohama City University, 3-9 FukuuraKanazawa-ku Yokohama 236-0004, Japan
e-mail: naomat@yokohama-cu.ac.jp
e-mail: hsaitsu@yokohama-cu.ac.jp

C. Ohba
e-mail: t116017g@yokohama-cu.ac.jp

K. Nishiyama
e-mail: kiyomim@yokohama-cu.ac.jp

Y. Tsurusaki
e-mail: tsurusak@yokohama-cu.ac.jp

M. Nakashima
e-mail: mnakashi@yokohama-cu.ac.jp

N. Miyake
e-mail: nmiyake@yokohama-cu.ac.jp

C. Ohba · Y. Suzuki · H. Doi · A. Tomita-Katsumoto · F. Tanaka
Department of Clinical Neurology and Stroke Medicine, Yokohama City University, Yokohama 236-0004, Japan

Y. Suzuki
e-mail: yume@med.yokohama-cu.ac.jp

H. Doi
e-mail: doi@rkd.d-bs.com

A. Tomita-Katsumoto
e-mail: chiwawan-atsuko@hotmail.co.jp

F. Tanaka
e-mail: ftanaka@yokohama-cu.ac.jp

H. Osaka · M. Iai · S. Yamashita
Division of Neurology, Kanagawa Children's Medical Center, Clinical Research Institute, Yokohama 232-0066, Japan

H. Osaka
e-mail: hosaka@kcmc.jp

Our data clearly demonstrate the utility of whole exome sequencing for genetic diagnosis of childhood cerebellar and/or vermis atrophy.

Keywords Cerebellar and/or vermis atrophy · Whole exome sequencing · De novo mutation · Compound heterozygous mutation

Introduction

Cerebellar atrophy in childhood can be classified into three types: hereditary cerebellar atrophy, postnatally acquired cerebellar atrophy, and unilateral cerebellar atrophy [1]. The number of differential diagnoses for hereditary cerebellar atrophy in childhood exceeds 70 diseases, the clinical findings of which often overlap with each other [1]. For example, ataxia was recognized as one of the main symptoms in 36 diseases, intellectual disability in 14 diseases, and epilepsy in 20 diseases [1].

In a review of 402 patients with cerebellar abnormality on magnetic resonance imaging (MRI), 66 patients showed posterior fossa malformation including Joubert syndrome [2]. Among 300 patients with cerebellar atrophy, in whom nongenetic etiologies were excluded, clinical diagnosis was established in 142 patients (47 %), and consisted of mitochondrial disorders (37 patients), neuronal ceroid lipofuscinosis (25 patients), ataxia telangiectasia (14 patients), and GM2 gangliosidosis (10 patients) [2]. The estimated prevalence of these disorders is rare, with reports of only 9.2 per 100,000 people affected with mitochondrial disorders in northeast England [3], 1.2 per 1,000,000 with neuronal ceroid lipofuscinosis in Italy [4], and 0.4 per 100,000 with ataxia telangiectasia in southeast Norway [5]. Therefore, clinical diagnosis of disorders with cerebellar abnormality is often difficult as many rare disorders with overlapping clinical features are included in this condition.

The genetic diagnosis of cerebellar and/or vermis atrophy is more challenging. Causative mutations for cerebellar atrophy and ataxia disorders have been found in more than 150 genes [1, 2, 6–8]. Joubert syndrome, which shows vermis atrophy/hypoplasia, is also genetically heterogeneous as mutations in 21 genes have been reported [7]. Whole exome sequencing (WES), which employs the targeted capture of protein encoding exons and massively parallel DNA sequencing, has enabled the comprehensive examination of mutations in more than 90 % of exons [9]. In addition, de novo or recessive mutations can be systemically identified by family-based exome sequencing using trios of a patient and his/her parents [10], suggesting that WES is useful for genetic diagnosis in heterogeneous genetic disorders. Indeed, family-based WES successfully detected disease-causing mutations in 16 of 100 patients with severe intellectual disability, which were both clinically and genetically heterogeneous [11].

In this study, we performed family-based WES in 23 families including 25 patients who showed cerebellar and/or vermis atrophy in childhood on a brain MRI. We successfully identified disease-causing mutations in nine families (9/23, 39.1 %).

Patients and methods

Patients

We analyzed 23 families including 25 patients with various degrees of cerebellar and/or vermis atrophy on brain MRI, and their unaffected parents and siblings (if available). All patients were sporadic, except for two who each had two affected siblings. Clinical examination failed to provide a clear diagnosis for each of the patients included in this study. Both static malformations and progressive cerebellar atrophy were included. Serum levels of lactic acid and pyruvate fell within the normal range for all patients. α-fetoprotein, total-cholesterol, and immunoglobulin levels were measured to exclude ataxia telangiectasia. Serum levels of albumin and tocopherol were examined in 23 of 25 patients, excluding early-onset ataxia with oculomotor apraxia and hypoalbuminemia, and ataxia with isolated vitamin E deficiency, respectively (Supplementary Table 1). Genomic DNA was isolated from peripheral blood leukocytes using QuickGene 610 L

M. Iai
e-mail: miai@kcmc.jp

S. Yamashita
e-mail: syamashita@kcmc.jp

N. Aida
Division of Radiology, Kanagawa Children's Medical Center, Clinical Research Institute, Yokohama 232-0066, Japan
e-mail: naida@kcmc.jp

N. Shimozawa
Division of Genomics Research, Life Science Research Center, Gifu University, Gifu 501-1193, Japan
e-mail: nshim@gifu-u.ac.jp

A. Takamura · Y. Eto
Department of Genetics and Genome Science, Tokyo Jikei University School of Medicine, Tokyo 105-8461, Japan

A. Takamura
e-mail: ayumi.takamura@mt.strins.or.jp

Y. Eto
e-mail: yosh@sepia.ocn.ne.jp

A. Takamura · Y. Eto
Advanced Clinical Research Center, Institute of Neurological Disorders, Kawasaki 215-0026, Japan

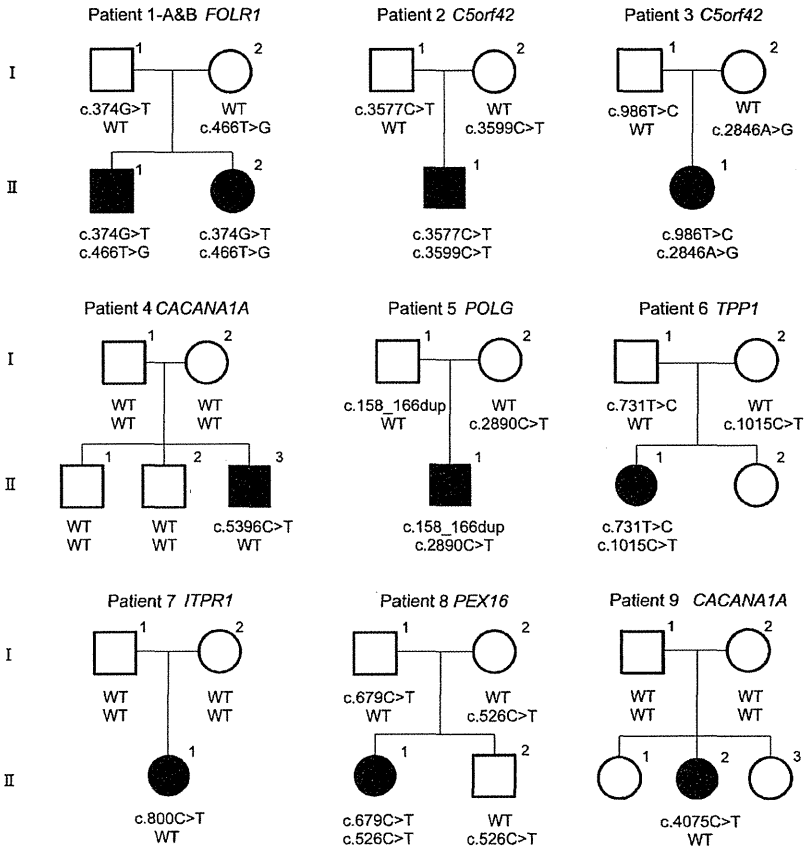

Fig. 1 Pedigrees of nine kindreds with cerebellar atrophy in childhood. Causative mutations were identified in seven genes. The segregation of each mutation is shown

(Wako, Osaka, Japan). The Institutional Review Board of Yokohama City University School of Medicine approved the experimental protocols. Informed consent was obtained for all individuals included in this study in agreement with the requirements of Japanese regulations.

Whole exome sequencing

Genomic DNA was captured using the SureSelect Human All Exon v4 Kit (51 Mb; Agilent Technologies, Santa Clara, CA, USA) and sequenced on an Illumina HiSeq2000 (Illumina, San Diego, CA, USA) with 101 bp paired-end reads. Four samples were run in one lane of the flow cell. Exome data processing, variant calling, and variant annotation were performed as previously described [12].

Results

Family-based WES was performed in 23 families including 25 patients and their unaffected parents and siblings. The average read depth of the protein-coding regions of RefSeq genes was 124.50 (range across all samples, 81.85–185.67), such that 94.3 % of targeted coding sequences was covered by 10 reads or more. We filtered out common single nucleotide polymorphisms (SNPs) that met the following two criteria: variants showing minor allele frequencies ≥1% in dbSNP 135 and variants found in more than two of our in-house 406 control exomes. Protein-altering and splicing-affecting variants were considered for downstream analysis. Mutations in previously reported causative genes for cerebellar atrophy were examined with particular attention (Supplementary Table 1).

All genes were surveyed for de novo mutations and compound heterozygous or homozygous mutations in each family. We identified pathological mutations in seven genes within nine families (9/23, 39.1%): compound heterozygous *FOLR1* mutations in patients 1A and 1B (siblings) [c.374G>T (p.R125L) and c.466T>G (p.W156G)]; a de novo *CACNA1A* mutation in patients 4 and 9 [c.5396C>T (p.S1799L) and c.4075C>T (p.R1359W)], respectively; compound heterozygous *C5orf42* mutations in patients 2 and 3 [c.3577C>T(p.R1193C) and c.3599C>T (p.A1200V) in patient 2, c.986T>C (p.L329P) and c.2846A>G (p.Y949C) in patient 3]; compound heterozygous *POLG* mutations in patient 5 [c.158_166dup (p.Q53_Q55dup) and c.2890C>T (p.R964C)]; compound heterozygous *TPP1* mutations in patient 6 [c.731T>C (p.M244T) and c.1015C>T (p.R339W)]; a de novo *ITPR1* mutation in patient 7 [c.800C>T (p.T267M)]; and compound heterozygous *PEX16* mutations in patient 8 [c.679C>T (p.R227W) and c.526C>T (p.R176*)] (Fig. 1 and Table 1). These mutations were confirmed by Sanger

Table 1 Clinical features of patients

Patient number	1-A	1-B	2	3	4	5	6	7	8	9
Age (years), gender	17 years, male	14 years, female	5 years, male	2 years, female	8 years, male	8 years, male	5 years, female	6 years, female	9 years, female	20 years, female
Gene mutated	*FOLR1*	*FOLR1*	*C5orf42*	*C5orf42*	*CACNA1A*	*POLG*	*TPP1*	*ITPR1*	*PEX16*	*CACNA1A*
Known disease(s) caused by mutations	Neurodegeneration from cerebral folate transport deficiency	Neurodegeneration from cerebral folate transport deficiency	Joubert syndrome	Joubert syndrome	SCA6, Episodic ataxia type 2, FHM1	mtDNA depletion syndrome, Mitochondrial recessive ataxia syndrome, PEO	Neuronal ceroid lipofuscinosis type2, autosomal recessive spinocerebellar ataxia type 7	SCA15, SCA29	Zellweger syndrome	SCA6, Episodic ataxia type 2, FHM1
Mutations (number of control exomes harboring the mutation/total control exomes)	c.374G>T p.R125L (0/406) c.466T>G p.W156G (0/406)	c.374G>T p.R125L (0/406) c.466T>G p.W156G (0/406)	c.3577C>T p.R1193C (0/406) c.3599C>T p.A1200V (0/406)	c.986T>C p.L329P (0/406) c.2846A>G p.Y949C (0/406)	c.5396C>T p.S1799L (0/406)	c.158_166dup p.Q53_Q55dup (0/406) c.2890C>T[a] p.R964C (2/406)	c.731T>C p.M244T (0/406) c.1015C>T p.R339W (0/406)	c.800C>T p.T267-M (0/406)	c.679C>T p.R227W (0/406) c.526C>T[a] p.R176* (0/406)	c.4075C>T p.-R1359-W (0/406)
Inheritance	Compound heterozygous	Compound heterozygous	Compound heterozygous	Compound heterozygous	De novo	Compound heterozygous	Compound heterozygous	De novo	Compound heterozygous	De novo
Initial symptom	Ataxic gait	Ataxic gait	Developmental delay	Hypotonia	Developmental delay	Hypotonia	Epilepsy	Hypotonia/nystagmus	Ataxic gait	Epilepsy
Age at onset	1 years	2 years	9 months	1 years	9 months	6 months	3 years	4 months	1 years	3 months
Ataxia	+	+	−	+	+	+	+	+	+	+
Dysmetria	−	−	−	−	+	−	+	−	+	+
Oculomotor apraxia	−	−	+	+	+	−	−	−	+	+
Intention tremor	+	+	−	−	+	−	−	+	+	+
Other	Slurred speech	Slurred speech					Slurred speech	Nystagmus/slurred speech	Slurred speech	Slurred speech
Developmental delay	+	+	+	+	+	+	+	+	+	+
Intellectual disability	+	+	+	+	+	+	+	+	−	+
Speech ability	Three-word sentences	Three-word sentences	Two-word sentences	Two-word sentences	Few words	N.D.	Three-word sentences	Three-word sentences	Few words	Few words
Muscle tone	Mild hypotonia/spastic lower limbs	Mild hypotonia	Hypotonia	Hypotonia	Hypotonia	Hypotonia	−	Hypotonia	Hypotonia	Hypotonia
Pyramidal sign	+	−	−	−	−	−	−	−	−	+ (DTR↑)
Extrapyramidal sign	−	−	−	−	−	−	−	−	−	−
Peripheral neuropathy	−	N.D.	N.D	N.D.	−	N.D.	N.D.	N.D.	−	−
Epileptic seizure	+	+	−	−	+	−	+	−	−	+
Complication	Low IgG			Aortic coarctation					Pigmentary retinal	

Table 1 (continued)

Patient number	1-A	1-B	2	3	4	5	6	7	8	9
MRI									degeneration	
Cerebellar atrophy/ hypoplasia	+	+	Vermis atrophy	Vermis hypoplasia	+	+	+	+	+ (mild)	+
Brainstem atrophy	+ (mild)	–	–	–	–	–	–	–	–	–
Other	Cerebral WM atrophy, Calcification at subcortical WM	Calcification at basal ganglia and subcortical WM	Molar tooth sign							

WM white matter, *PEO* progressive external ophthalmoplegia, *FHM1* familial hemiplegic migraine type1, *mtDNA* mitochondrial DNA, *DTR* deep tendon reflex, *N.D.* not detected

[a] This mutation has been previously reported as disease-causing

sequencing. Five of 15 mutations were registered in dbSNP (http://www.ncbi.nlm.nih.gov/projects/SNP/) as rare variants (Supplementary Table 2). None of the mutations were present in the 6,500 exomes sequenced by the National Heart, Lung, and Blood Institute exome project or our 406 in-house control exomes, except for c.2890C>T in *POLG*, which was found in 2 of 406 control exomes (Table 1, and Supplementary Table 2). Two mutations (c.2890C>T in *POLG* and c.526C>T in *PEX16*) have been reported as disease-causing mutations [13, 14]. All of the single nucleotide substitutions (SNVs) occurred at evolutionally conserved amino acids (as shown by high PhyloP score), and Sorting Intolerant From Tolerant (SIFT), Polyphen2, and Mutation Taster predicted that all the SNVs would be highly damaging to the protein structure (Supplementary Table 2), supporting pathogenicity of the mutations.

Clinical features of the ten patients are summarized in Table 1 (see also supplementary Case report). All patients exhibited motor developmental delay (10/10, 100%), and nine patients had an intellectual disability (9/10, 90%). All patients showed cerebellar signs (10/10, 100%) such as ataxia of the limbs and trunk, oculomotor apraxia, dysmetria, intention tremor, slurred speech and nystagmus. Hypotonia and epileptic seizures were observed in nine and five patients, respectively (9/10, 90%; 5/10, 50%). Patient 1B with compound heterozygous *FOLR1* mutations, which cause neurodegeneration from cerebral folate transport deficiency [15, 16], showed an extremely low concentration of 5-methyltetrahydrofolate (5-MTHF) in the cerebrospinal fluid and serum (0.0 nmol/l and 5.0 nmol/l). In patient 6 with compound heterozygous *TPP1* mutations, markedly low activity of tripeptidyl peptidase 1 was observed: 5.44 nmol/mg/h in leukocytes and 0.092 pmol/punch/h in dried blood spot (Supplementary Table 3) [17, 18]. Patient 8 with compound heterozygous *PEX16* mutations showed mildly increased very long chain fatty acids (VLCFAs) as previously described [19, 20]: C24:0/C22:0 1.15 [average 1.05, standard deviation (SD) 0.16], C25:0/C22:0 0.035 (average 0.024, SD 0.006), and C26:0/C22:0 0.038 (average 0.012, SD 0.005). Plasmalogen and phytanic acid were within normal range (data not shown). Brain MRI (Fig. 2) revealed cerebellar atrophy (both hemispheres and vermis) in eight patients (8/10, 80%), vermis atrophy/hypoplasia in two patients (2/10, 20%), and brainstem atrophy in one patient (1/10, 10%). Abnormal signal in the white matter was not observed in sibling patients 1A and 1B, but patient 1A showed decreased white matter volume (Fig. 2c). Calcification was recognized in the subcortical matter (patients 1A and 1B) and basal ganglia (patient 1B) (Fig. 2d). Molar tooth sign, which is a characteristic feature of Joubert syndrome, was observed in patient 2 with *C5orf42* mutations (Fig. 2f). Brain MRI in patient 3 with *C5orf42* mutations showed vermis hypoplasia, but no clear molar tooth sign as deepened interpeduncular fossa, secondary distortion and enlargement of the fourth ventricle, and horizontally oriented superior

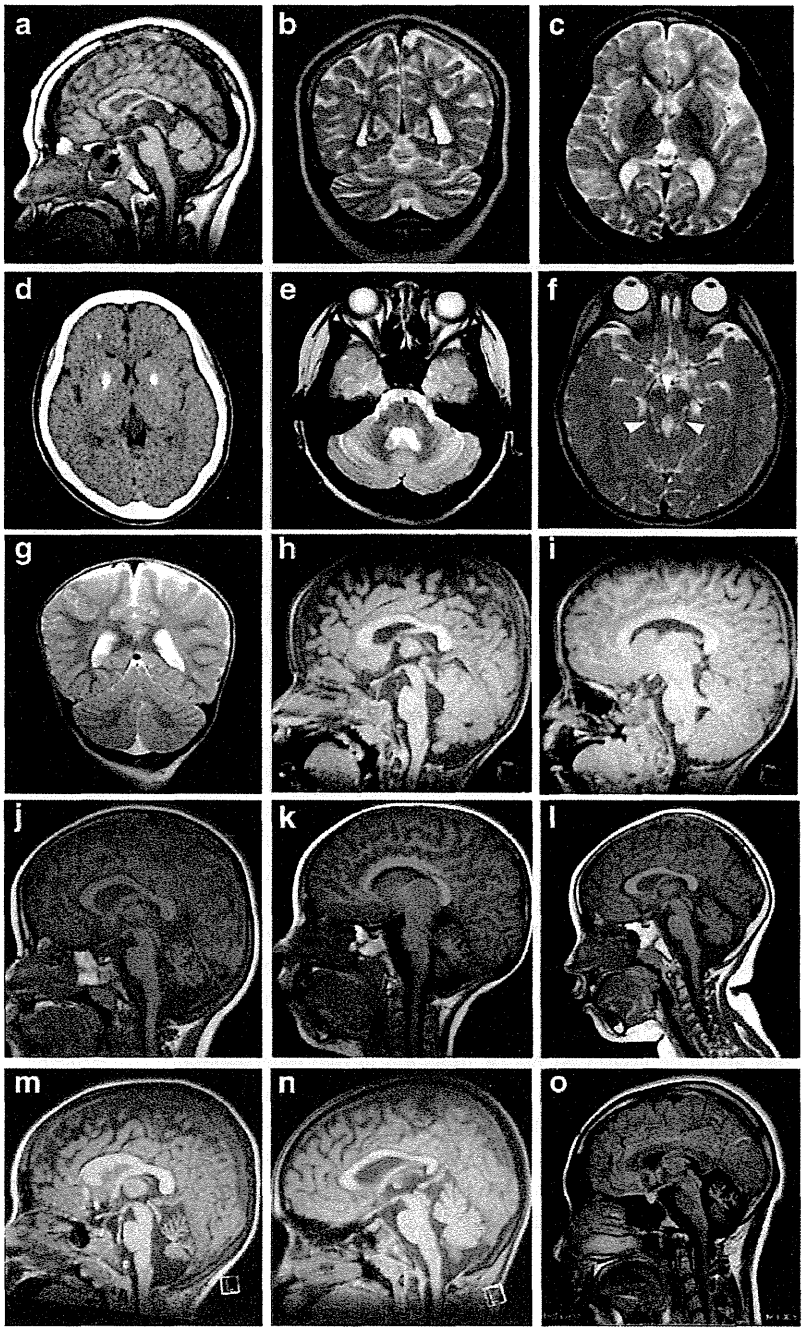

Fig. 2 **a**, **h**–**o** T1-weighted midline sagittal images, **b**, **g** T2-weighted coronal images, **c**, **e**, **f** T2-weighted axial images, **d** computed tomography images of the patients (**a**, **b**, **c**, patient 1A at 8 years of age; **d**, **e**, patient 1B at 12 years; **f**, patient 2 at 1 year and 8 months; **g**, **h**, **i** patient 3 at 1 year and 5 months; **j** patient 4 at 3 years; **k** patient 5 at 4 years; **l** patient 6 at 4 years; **m** patient 7 at 5 years; **n** patient 8 at 8 years; **o** patient 9 at 20 years). Vermis atrophy was observed in all patients (**b**, **e**, **f**, **g**, **j**–**o**) and very mild brain stem atrophy (especially in the basilar part of the pons) in patient 1A (**a**). In patient 1A, decreased volume but no abnormal signal in the white matter was observed (**c**). Calcification was observed in the subcortical white matter and basal ganglia of patient 1B (**d**). Patient 2 showed molar tooth sign (**f**, *arrowhead*), patient 3 showed vermis hypoplasia (**g**), but molar tooth sign was unclear as deepened interpeduncular fossa, secondary distortion and enlargement of the fourth ventricle, and horizontally oriented superior cerebellar peduncles were only mildly observed, with lack of thickened and elongated superior cerebellar peduncles (**h**, **i**)

cerebellar peduncles were only mildly observed, with lack of thickened and elongated superior cerebellar peduncles (Fig. 2g–i).

Discussion

In this report, the genetic basis of disorders showing cerebellar and/or vermis atrophy in childhood was successfully clarified in 9 of 23 families (39.1 %). Of note, mutations in seven distinct genes were identified, further supporting clinical and genetic heterogeneity of this condition. By family-based exome sequencing, we readily found three de novo mutations and six compound heterozygous mutations during a short period of time, demonstrating that family-based WES, when used with ethnically matched normal control exome data for prioritizing variants, is extremely powerful for dissecting genetic basis of neurological genetic disorders.

It is important to carefully address the relevance of identified mutations in respective cases by evaluating clinical information compared with previous reports and biochemical examination. Zellweger syndrome caused by *PEX16* mutations has been reported to show a very severe clinical course and white matter abnormalities [21]. Although patient 8 with *PEX16* mutations showed no white matter abnormalities and mild clinical features, Ebberink et al. recently reported patients with *PEX16* mutations, showing an atypical mild phenotype similar to our patient [19]. In addition, elevated VLCFAs levels, which are characteristic for *PEX16* mutations, were observed in our patient, supporting the notion that the identified *PEX16* mutations cause a relatively mild phenotype. Neuronal ceroid lipofuscinosis 2 caused by *TPP1* mutations is characterized by epilepsy, loss of vision, ataxia, and rapid progression [22]. Recently, Sun et al. showed that *TPP1* mutations can cause autosomal recessive SCAR7, which shows ataxia and low activity of tripeptidyl peptidase 1 [23]. Patient 6 with *TPP1* mutations showed epilepsy, ataxia, and low activity of tripeptidyl peptidase 1, suggesting that the phenotype was within the clinical spectrum caused by *TPP1* mutations.

De novo *CACNA1A* mutations were identified in patients 4 and 9, who showed no episodic ataxia or hemiplegia, a known phenotype caused by *CACNA1A* mutation [24]. However, cerebellar atrophy is a common feature of patients with *CACNA1A* mutations, and CAG repeat expansion in *CACNA1A* causes spinocerebellar ataxia type 6 (SCA6). In addition, the occurrence of de novo mutations has been estimated to be 7.6×10^{-9} and 2.2×10^{-8} per nucleotide in diploid embryos, suggesting that an average newborn is expected to acquire approximately 0.86 amino acid-altering mutations [25, 26]. Therefore, the chance coexistence of cerebellar atrophy and a de novo *CACNA1A* mutation in two independent patients is extremely rare, suggesting causal relationship between *CACNA1A* mutation and cerebellar atrophy. Haploinsufficiency of *ITPR1* was reported to cause adult-onset SCA15 associated with a slowly progressive pure type of cerebellar ataxia [27]. However, Huang et al. recently found that missense mutations in *ITPR1* caused infantile-onset SCA29 in two families, which is characterized by delayed motor development, cognitive delay, and cerebellar ataxia with cerebellar atrophy in a brain MRI [28]. The clinical features of our patient 7 with a de novo missense mutation in *ITPR1* is consistent with SCA29, confirming that *ITPR1* missense mutations can cause infantile-onset cerebellar atrophy.

We identified *C5orf42* mutations in patients 2 and 3 with vermis atrophy/hypoplasia. Molar tooth sign in brain MRI has been reported in patients with *C5orf42* mutations [29]. Although both patients showed hypotonia, developmental delay, mental retardation and oculomotor apraxia [30], characteristic molar tooth sign was only observed in patient 2. Therefore, retrospectively, patient 2 should be diagnosed with Joubert syndrome, but diagnosis of Joubert syndrome in patient 3 was challenging with no molar tooth sign. WES was able to provide correct genetic diagnosis in such atypical cases. Of note, in patients 1A and 1B with *FOLR1* mutations, folate deficiency can be improved with oral folinic acid administration [15, 16]. Therefore, genetic investigation by WES together with careful clinical evaluation will enhance correct diagnosis of patients, and may benefit their clinical management.

Acknowledgments We would like to thank all patients and their families for their participation in this study. We also thank Aya Narita and Nobuko Watanabe for technical assistance. This work was supported by the Ministry of Health, Labour, and Welfare of Japan; the Japan Society for the Promotion of Science (a Grant-in-Aid for Scientific Research (B) from (25293085, 25293235), a Grant-in-Aid for Scientific Research (A) (13313587)); the Takeda Science Foundation; the Japan Science and Technology Agency; the Strategic Research Program for Brain Sciences (11105137); and a Grant-in-Aid for Scientific Research on Innovative Areas (Transcription Cycle) from the Ministry of Education, Culture, Sports, Science, and Technology of Japan (12024421).

References

1. Poretti A, Wolf NI, Boltshauser E (2008) Differential diagnosis of cerebellar atrophy in childhood. Eur J Paediatr Neurol 12(3):155–167. doi:10.1016/j.ejpn.2007.07.010
2. Al-Maawali A, Blaser S, Yoon G (2012) Diagnostic approach to childhood-onset cerebellar atrophy: a 10-year retrospective study of 300 patients. J Child Neurol 27(9):1121–1132. doi:10.1177/0883073812448680
3. Schaefer AM, McFarland R, Blakely EL, He L, Whittaker RG, Taylor RW, Chinnery PF, Turnbull DM (2008) Prevalence of mitochondrial DNA disease in adults. Ann Neurol 63(1):35–39. doi:10.1002/ana.21217
4. Santorelli FM, Garavaglia B, Cardona F, Nardocci N, Bernardina BD, Sartori S, Suppiej A, Bertini E, Claps D, Battini R, Biancheri R, Filocamo M, Pezzini F, Simonati A (2013) Molecular epidemiology of childhood neuronal ceroid-lipofuscinosis in Italy. Orphanet J Rare Dis 8:19. doi:10.1186/1750-1172-8-19
5. Erichsen AK, Koht J, Stray-Pedersen A, Abdelnoor M, Tallaksen CM (2009) Prevalence of hereditary ataxia and spastic paraplegia in southeast Norway: a population-based study. Brain 132(Pt 6):1577–1588. doi:10.1093/brain/awp056
6. Matilla-Duenas A (2012) The ever expanding spinocerebellar ataxias. Editorial Cerebellum 11(4):821–827. doi:10.1007/s12311-012-0376-4
7. Valente EM, Brancati F, Boltshauser E, Dallapiccola B (2013) Clinical utility gene card for: Joubert syndrome—update 2013. Eur J Hum Genet. doi:10.1038/ejhg.2013.10
8. Vermeer S, van de Warrenburg BP, Willemsen MA, Cluitmans M, Scheffer H, Kremer BP, Knoers NV (2011) Autosomal recessive cerebellar ataxias: the current state of affairs. J Med Genet 48(10):651–659. doi:10.1136/jmedgenet-2011-100210
9. Bamshad MJ, Ng SB, Bigham AW, Tabor HK, Emond MJ, Nickerson DA, Shendure J (2011) Exome sequencing as a tool for Mendelian disease gene discovery. Nat Rev Genet 12(11):745–755. doi:10.1038/nrg3031
10. Vissers LE, de Ligt J, Gilissen C, Janssen I, Steehouwer M, de Vries P, van Lier B, Arts P, Wieskamp N, del Rosario M, van Bon BW, Hoischen A, de Vries BB, Brunner HG, Veltman JA (2010) A de

novo paradigm for mental retardation. Nat Genet 42(12):1109–1112. doi:10.1038/ng.712

11. de Ligt J, Willemsen MH, van Bon BW, Kleefstra T, Yntema HG, Kroes T, Vulto-van Silfhout AT, Koolen DA, de Vries P, Gilissen C, del Rosario M, Hoischen A, Scheffer H, de Vries BB, Brunner HG, Veltman JA, Vissers LE (2012) Diagnostic exome sequencing in persons with severe intellectual disability. N Engl J Med 367(20): 1921–1929. doi:10.1056/NEJMoa1206524
12. Saitsu H, Nishimura T, Muramatsu K, Kodera H, Kumada S, Sugai K, Kasai-Yoshida E, Sawaura N, Nishida H, Hoshino A, Ryujin F, Yoshioka S, Nishiyama K, Kondo Y, Tsurusaki Y, Nakashima M, Miyake N, Arakawa H, Kato M, Mizushima N, Matsumoto N (2013) *De novo* mutations in the autophagy gene *WDR45* cause static encephalopathy of childhood with neurodegeneration in adulthood. Nat Genet. doi:10.1038/ng.2562
13. Yamanaka H, Gatanaga H, Kosalaraksa P, Matsuoka-Aizawa S, Takahashi T, Kimura S, Oka S (2007) Novel mutation of human DNA polymerase gamma associated with mitochondrial toxicity induced by anti-HIV treatment. J Infect Dis 195(10):1419–1425. doi:10.1086/513872
14. Honsho M, Tamura S, Shimozawa N, Suzuki Y, Kondo N, Fujiki Y (1998) Mutation in PEX16 is causal in the peroxisome-deficient Zellweger syndrome of complementation group D. Am J Hum Genet 63(6):1622–1630. doi:10.1086/302161
15. Grapp M, Just IA, Linnankivi T, Wolf P, Lucke T, Hausler M, Gartner J, Steinfeld R (2012) Molecular characterization of folate receptor 1 mutations delineates cerebral folate transport deficiency. Brain 135(Pt 7):2022–2031. doi:10.1093/brain/aws122
16. Steinfeld R, Grapp M, Kraetzner R, Dreha-Kulaczewski S, Helms G, Dechent P, Wevers R, Grosso S, Gartner J (2009) Folate receptor alpha defect causes cerebral folate transport deficiency: a treatable neurodegenerative disorder associated with disturbed myelin metabolism. Am J Hum Genet 85(3):354–363. doi:10.1016/j.ajhg.2009.08.005
17. Lukacs Z, Santavuori P, Keil A, Steinfeld R, Kohlschutter A (2003) Rapid and simple assay for the determination of tripeptidyl peptidase and palmitoyl protein thioesterase activities in dried blood spots. Clin Chem 49(3):509–511
18. Sohar I, Lin L, Lobel P (2000) Enzyme-based diagnosis of classical late infantile neuronal ceroid lipofuscinosis: comparison of tripeptidyl peptidase I and pepstatin-insensitive protease assays. Clin Chem 46(7):1005–1008
19. Ebberink MS, Csanyi B, Chong WK, Denis S, Sharp P, Mooijer PA, Dekker CJ, Spooner C, Ngu LH, De Sousa C, Wanders RJ, Fietz MJ, Clayton PT, Waterham HR, Ferdinandusse S (2010) Identification of an unusual variant peroxisome biogenesis disorder caused by mutations in the *PEX16* gene. J Med Genet 47(9):608–615. doi:10.1136/jmg.2009.074302
20. Shimozawa N, Nagase T, Takemoto Y, Suzuki Y, Fujiki Y, Wanders RJ, Kondo N (2002) A novel aberrant splicing mutation of the *PEX16* gene in two patients with Zellweger syndrome. Biochem Biophys Res Commun 292(1):109–112
21. Steinberg SJ, Dodt G, Raymond GV, Braverman NE, Moser AB, Moser HW (2006) Peroxisome biogenesis disorders. Biochim Biophys Acta 1763(12):1733–1748. doi:10.1016/j.bbamcr.2006.09.010
22. Kousi M, Lehesjoki AE, Mole SE (2012) Update of the mutation spectrum and clinical correlations of over 360 mutations in eight genes that underlie the neuronal ceroid lipofuscinoses. Hum Mutat 33(1):42–63. doi:10.1002/humu.21624
23. Sun Y, Almomani R, Breedveld GJ, Santen GW, Aten E, Lefeber DJ, Hoff JI, Brusse E, Verheijen FW, Verdijk RM, Kriek M, Oostra B, Breuning MH, Losekoot M, den Dunnen JT, van de Warrenburg BP, Maat-Kievit AJ (2013) Autosomal recessive spinocerebellar ataxia 7 (SCAR7) is caused by variants in TPP1, the gene involved in classic late-infantile neuronal ceroid lipofuscinosis 2 disease (CLN2 disease). Hum Mutat 34(5):706–713. doi:10.1002/humu.22292
24. Haan J, Terwindt GM, van den Maagdenberg AM, Stam AH, Ferrari MD (2008) A review of the genetic relation between migraine and epilepsy. Cephalalgia 28(2):105–113. doi:10.1111/j.1468-2982.2007.01460.x
25. Roach JC, Glusman G, Smit AF, Huff CD, Hubley R, Shannon PT, Rowen L, Pant KP, Goodman N, Bamshad M, Shendure J, Drmanac R, Jorde LB, Hood L, Galas DJ (2010) Analysis of genetic inheritance in a family quartet by whole-genome sequencing. Science 328(5978):636–639. doi:10.1126/science.1186802
26. Lynch M (2010) Rate, molecular spectrum, and consequences of human mutation. Proc Natl Acad Sci U S A 107(3):961–968. doi:10.1073/pnas.0912629107
27. Durr A (2010) Autosomal dominant cerebellar ataxias: polyglutamine expansions and beyond. Lancet Neurol 9(9):885–894. doi:10.1016/s1474-4422(10)70183-6
28. Huang L, Chardon JW, Carter MT, Friend KL, Dudding TE, Schwartzentruber J, Zou R, Schofield PW, Douglas S, Bulman DE, Boycott KM (2012) Missense mutations in *ITPR1* cause autosomal dominant congenital nonprogressive spinocerebellar ataxia. Orphanet J Rare Dis 7:67. doi:10.1186/1750-1172-7-67
29. Srour M, Schwartzentruber J, Hamdan FF, Ospina LH, Patry L, Labuda D, Massicotte C, Dobrzeniecka S, Capo-Chichi JM, Papillon-Cavanagh S, Samuels ME, Boycott KM, Shevell MI, Laframboise R, Desilets V, Maranda B, Rouleau GA, Majewski J, Michaud JL (2012) Mutations in *C5ORF42* cause Joubert syndrome in the French Canadian population. Am J Hum Genet 90(4):693–700. doi:10.1016/j.ajhg.2012.02.011
30. Parisi MA, Doherty D, Chance PF, Glass IA (2007) Joubert syndrome (and related disorders) (OMIM 213300). Eur J Hum Genet 15(5):511–521. doi:10.1038/sj.ejhg.5201648

Journal of Human Genetics (2013) 58, 822–824

www.nature.com/jhg

SHORT COMMUNICATION

Novel *FIG4* mutations in Yunis–Varon syndrome

Junya Nakajima[1,2], Nobuhiko Okamoto[3], Jun Shiraishi[4], Gen Nishimura[5], Mitsuko Nakashima[1], Yoshinori Tsurusaki[1], Hirotomo Saitsu[1], Hisashi Kawashima[2], Naomichi Matsumoto[1] and Noriko Miyake[1]

Yunis–Varon syndrome (YVS, MIM 216340) is a rare autosomal recessive disorder characterized by skeletal abnormalities and severe neurological impairment with vacuolation of the central nervous system, skeletal muscles and cartilages. Very recently, mutations of the *FIG4* (FIG4 homolog, SAC1 lipid phosphatase domain containing (*Saccharomyces cerevisiae*)) gene, which encodes a 5′-phosphoinositide phosphatase essential for endosome/lysosome function have been identified as the cause for YVS. Interestingly, *FIG4* mutations were previously reported to be responsible for other neurodegenerative diseases such as autosomal recessive Charcot–Marie–Tooth disease type 4J and autosomal dominant amyotrophic lateral sclerosis/primary lateral sclerosis. We analyzed a YVS patient using whole-exome sequencing, and identified novel biallelic *FIG4* mutations: c.1750+1delG and c.2284_2285delCT (p.S762Wfs*3). These two mutations were mutations supposed to have null function. To our knowledge, this is the second report of *FIG4* mutations in YVS and our result supports the idea that biallelic null mutations of *FIG4* cause YVS in human.
Journal of Human Genetics (2013) **58**, 822–824; doi:10.1038/jhg.2013.104; published online 3 October 2013

Keywords: biallelic mutation; *FIG4*; whole-exome sequencing; Yunis–Varon syndrome

Yunis–Varon syndrome (YVS, MIM_216340) is a rare autosomal recessive disorder characterized by skeletal abnormalities (cleidocranial dysostosis, bilateral absence of thumbs and halluces distal aphalangia and pelvic bone dysplasia) and severe neurological impairment.[1] Recently, mutations of *FIG4* (FIG4 homolog, SAC1 lipid phosphatase domain containing (*Saccharomyces cerevisiae*); NM_014845.5) were identified as the genetic cause for YVS.[2] *FIG4* encodes FIG4 protein (also known as SAC3) which is a 5′-phosphoinositide phosphatase essential for endosome/lysosome function.[3] FIG4 binds with Vac14/ArPIKfyve and Fab1/PIKfyve to form a functional complex on early endosomal membranes known as PIKfyve–ArPIKfyve–Sac3 complex.[3] The PIKfyve–ArPIKfyve–Sac3 complex mediates the conversion of endosomal phosphatidylinositol 3-phosphate (PI3P) to phosphatidylinositol 3,5-biphosphate ($PI(3,5)P_2$), and this conversion is essential for protein sorting, trafficking late endosomes to lysosomal degradation compartment and regulating some other endolysosome/lysosome functions essential for degradation such as ion channel activation and endolysosome fusion/fission.[4] Impairment of FIG4 causes a reduction of $PI(3,5)P_2$, which results in the malfunction of the endosome/endolysosome/lysosome. Therefore, the accumulation of undegraded materials in these compartments leads to dilatation.[3]

FIG4 abnormalities were previously reported to be the causative for autosomal recessive Charcot–Marie–Tooth disease type 4J (CMT4J, MIM#611228) and autosomal dominant amyotrophic lateral sclerosis (ALS, MIM#105400)/primary lateral sclerosis (PLS, MIM#611637).[2,5–7] Vacuolated endolysosomes are found in the perinuclear regions of peripheral neurons of *Fig4*-null mice and CMT4J patients.[3] In YVS patients, vacuolation was observed in skeletal muscles, fibroblasts and the central nervous system including cerebral cortex, the basal ganglia, cerebellar olives and medullary olives.[8–10]

The patient was a 2-year-old girl at the time of genetic consultation. She was the second daughter of a nonconsanguineous pair of 32-year-old woman and a 25-year-old man. Both her parents and her sister were healthy. Fetal echogram revealed intrauterine growth retardation. She was born at 40 weeks of gestation, with Apgar scores of 2 and 1 at 1 and 5 min, respectively. Her birth weight was 3306 g (+0.6 SD), body length 52 cm (+1.5 SD) and head circumference 33 cm (−0.3 SD). Because of neonatal asphyxia, she was transferred to neonatal intensive care unit and supported by mechanical ventilation. Lower anal atresia was found and colostomy was performed. Tube feeding was necessary because of poor feeding activity. Tracheostomy was placed at 8 months of age because of severe respiratory impairment. She presented with characteristic face (protruding forehead, wide fontanels, temporal narrowing, hypertelorism, blepharophimosis, inverted epicanthus, flat nasal bridge, bilateral low set ears, short philtrum, high-arched palate, down-turned mouth,

[1]Department of Human Genetics, Yokohama City University Graduate School of Medicine, Yokohama, Japan; [2]Department of Pediatrics, Tokyo Medical University, Shinjuku, Japan; [3]Department of Medical Genetics, Osaka Medical Center and Research Institute for Maternal and Child Health, Izumi, Japan; [4]Department of Neonatal Medicine, Osaka Medical Center and Research Institute for Maternal and Child Health, Izumi, Japan and [5]Department of Radiology, Tokyo Metropolitan Children's Medical Center, Fuchu, Japan. Correspondence: Dr N Miyake or Dr N Matsumoto, Department of Human Genetics, Yokohama City University Graduate School of Medicine, Fukuura 3-9, Kanazawa-ku, Yokohama 236-0004, Japan.
E-mail: nmiyake@yokohama-cu.ac.jp or naomat@yokohama-cu.ac.jp
Received 27 June 2013; revised 31 August 2013; accepted 2 September 2013; published online 3 October 2013

micrognathia and sparse and depigmented scalp hair), hypoplasia of the right clavicle and other long bones, aplasia of the left clavicle, absence of bilateral thumbs and halluces, hypoplasia of the distal phalanges, multiple appendicular bone fracture and proctatresia (Figures 1a-c). Congenital cataract and hearing loss were also noted. Head computed tomography showed severe hypoplasia of the cerebrum and enlargement of lateral, third and fourth ventricles (Figure 1d). At the age of 2 years, her height was 67.4 cm (−4.9 SD), body weight was 9.1 kg (−1.9 SD) and head was circumference 46.2 cm (−0.2 SD). Her developmental mile stones were severely retarded. She was bedridden and unable to support her head. She was therefore diagnosed with YVS.

To identify the genetic cause of the proband, we performed whole-exome sequencing on the patient and her parents as *FIG4* mutations were not described in YVS when we started the genetic analysis. Peripheral blood samples were collected from the trio (patient and both parents) after obtaining written informed consent. This study was approved by the institutional review board of Yokohama City University School of Medicine. Each individual's DNA was captured with the SureSelect Human All Exon v4 Kit (Agilent Technologies, Santa Clara, CA, USA) and sequenced on a HiSeq2000 with 101 bp paired-end reads and 7 bp index reads (Illumina, San Diego, CA, USA). Image analysis and base calling were performed by sequence control software real-time analysis and CASAVA software v1.8 (Illumina). The reads were aligned to a human reference genome (hg19) with Novoalign 2.08.02 (http://www.novocraft.com/). After the removal of PCR duplication by Picard, the variants were called by Genome Analysis Toolkit 1.6-5 (GATK: http://www.broadinstitute.org/gatk/) and annotated by ANNOVAR (2012feb) (http://www.openbioinformatics.org/annovar/). Through this flow, common variants registered in common dbSNP137 (minor allele frequency $\geqslant 0.01$) (http://genome.ucsc.edu/cgi-bin/hgTrackUi?hgsid=335665349&c=chr6&g=snp137Common) were removed.

More than 93% of coding sequence was covered by at least 20 reads in each individual. Because this syndrome was suspected as an autosomal recessive disease because of the consanguinity and/or affected siblings in reported families,[1,11,12] we extracted homozygous or compound heterozygous variants using whole-exome sequencing data. Through data processing synonymous variants, variants in segmental duplications, variants registered in dbSNP137 or our in-house database (exome data of 408 Japanese individuals) were all excluded from the candidates (Figure 2). As a result, only one compound heterozygous mutation in *FIG4* remained: c.1750 + 1delG and c.2285_2286delCT (p.S762Wfs*3), which were also confirmed by Sanger sequencing. The c.1750 + 1delG at intron 15 and c.2283_2284delCT at exon 20 were inherited from her mother and father, respectively (Figure 3).

Campeau *et al.*[2] proposed a model in which the clinical difference among the above-mentioned three conditions regarding *FIG4* abnormalities (that is, YVS, CMT4J and ALS/PLS) depends on how much residual FIG4 function remains based on the following evidence: (1) all previously reported CMT4J patients had compound heterozygous mutations but carried one null allele and one missense allele, whereas all YVS patients had biallelic null mutations.[7,13–15] (2) ALS/PLS patients had heterozygous null or partially loss-of-function mutations.[5] (3) In functional assays,

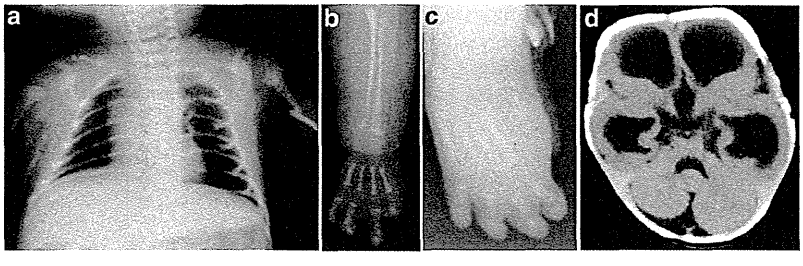

Figure 1 Imaging studies of the proband. (**a**) Thoracoabdominal X-ray on the first day after birth (dorsal position). Hypoplasia of both clavicle and the fracture of left humerus were evident. (**b**) X-ray of left forearm and hand. Absence of thumbs and hypoplastic phalangeal bones were observed. (**c**) X-ray of right foot. Absence of halluces and hypoplastic phalangeal bones was noted. (**d**) Head CT. Extended hypoplasia of the cerebrum and enlargement of the third and the lateral ventricles were noted. The fourth ventricle was also slightly enlarged.

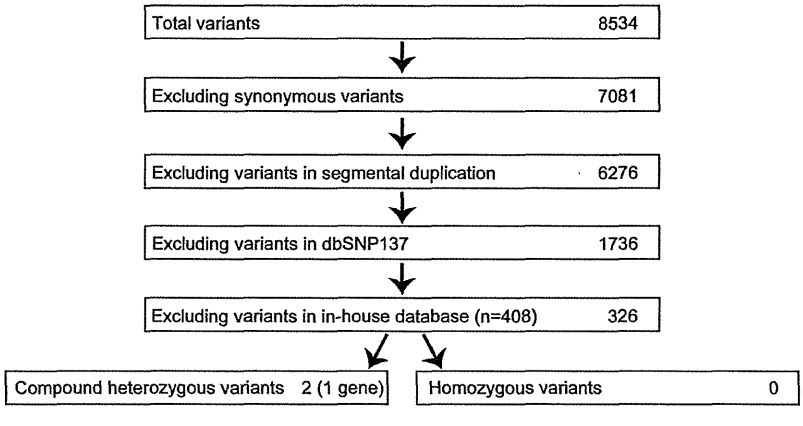

Figure 2 Priority scheme of whole-exome sequencing data. Numbers of variants surviving after each selection are shown.

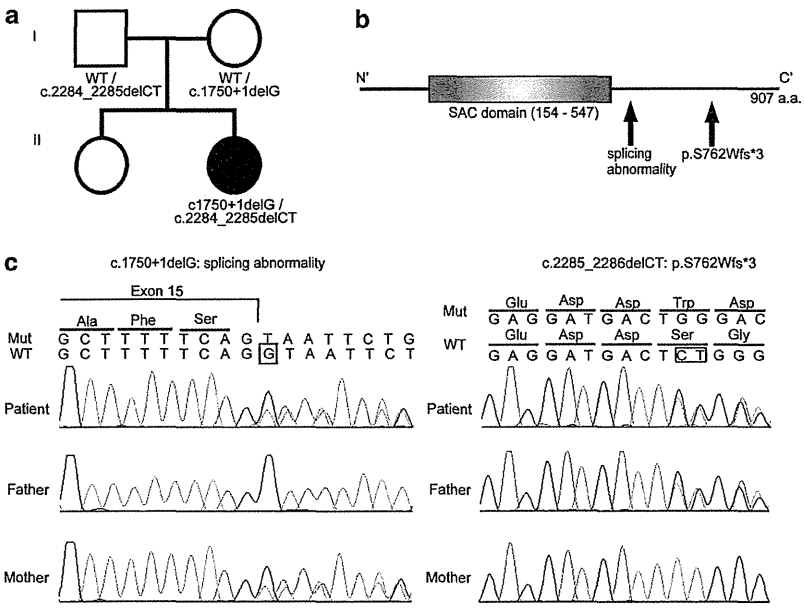

Figure 3 *FIG4* mutations in the patient. (**a**) Pedigree and mutations. (**b**) Schematic presentation of the FIG4 protein and mutations found in the patient. (**c**) Electropherograms corresponding to each mutation in the patient, her father and mother. WT: wild-type allele, Mut: mutant allele. The altered or deleted bases were marked by square.

CMT4J patients had less FIG4 activity than ALS/PLS patients.[5] Biallelic null mutations in our YVS patient support this model.

The clinical effects of heterozygous *FIG4* mutations remain unclear. Theoretically, all parents (excluding the patient having a *de novo* truncation mutation) of YVS patients should carry a heterozygous null mutation. However, none of the parents of identified CMT4J patients or YVS patients, who should be heterozygous carriers, have been reported to show ALS/PLS. The current age of the father and mother in this study were 27 and 34 years old, respectively, and they did not show any ALS/PLS phenotype. Furthermore, the patient's grandparents did not show any sign of ALS/PLS. This discrepancy could be presymptomatic status of the family members carrying a heterozygous mutation as the average onset age of ALS/PLS in patients with *FIG4* mutation was reported to be 56 ± 14 years (mean $\pm$ SD).[5] It would be strongly encouraged to observe their longitudinal clinical course of heterozygous carriers in human. The other possibility for this discrepancy would be unknown genetic modifier(s) leading to the incomplete penetrance. To clarify the genotype–phenotype correlation and the diverse clinical phenotypes by *FIG4* mutations, further studies of genetic and clinical features are necessary.

ACKNOWLEDGEMENTS

We thank the patient and her family for participating in this work. We also thank Ms S Sugimoto and K Takabe for their technical assistance. This work was supported by research grants from the Ministry of Health, Labour and Welfare (N Matsumoto and N Miyake), the Japan Science and Technology Agency (N Matsumoto), the Strategic Research Program for Brain Sciences (N Matsumoto) and a Grant-in-Aid for Scientific Research on Innovative Areas-(Transcription cycle)-from the Ministry of Education, Culture, Sports, Science and Technology of Japan (N Matsumoto), a Grant-in-Aid for Scientific Research from Japan Society for the Promotion of Science (H Saitsu, N Matsumoto and N Miyake), the Takeda Science Foundation (N Matsumoto and N Miyake) and the Hayashi Memorial Foundation for Female Natural Scientists (N Miyake).

1 Yunis, E. & Varon, H. Cleidocranial dysostosis, severe micrognathism, bilateral absence of thumbs and first metatarsal bone, and distal aphalangia: a new genetic syndrome. *Am. J. Dis. Child.* **134,** 649–653 (1980).
2 Campeau, P. M., Lenk, G. M., Lu, J. T., Bae, Y., Burrage, L., Turnpenny, P. *et al.* Yunis–Varon syndrome is caused by mutations in FIG4, encoding a phosphoinositide phosphatase. *Am. J. Hum. Genet.* **92,** 781–791 (2013).
3 Martyn, C. & Li, J. Fig4 deficiency: a newly emerged lysosomal storage disorder? *Prog. Neurobiol.* **101-102,** 35–45 (2013).
4 Huotari, J. & Helenius, A. Endosome maturation. *EMBO J.* **30,** 3481–3500 (2011).
5 Chow, C. Y., Landers, J. E., Bergren, S. K., Sapp, P. C., Grant, A. E., Jones, J. M. *et al.* Deleterious variants of FIG4, a phosphoinositide phosphatase, in patients with ALS. *Am. J. Hum. Genet.* **84,** 85–88 (2009).
6 Zhang, X., Chow, C. Y., Sahenk, Z., Shy, M. E., Meisler, M. H. & Li, J. Mutation of FIG4 causes a rapidly progressive, asymmetric neuronal degeneration. *Brain* **131,** 1990–2001 (2008).
7 Nicholson, G., Lenk, G. M., Reddel, S. W., Grant, A. E., Towne, C. F., Ferguson, C. J. *et al.* Distinctive genetic and clinical features of CMT4J: a severe neuropathy caused by mutations in the PI(3,5)P(2) phosphatase FIG4. *Brain* **134,** 1959–1971 (2011).
8 Garrett, C., Berry, A. C., Simpson, R. H. & Hall, C. M. Yunis–Varon syndrome with severe osteodysplasty. *J. Med. Genet.* **27,** 114–121 (1990).
9 Walch, E., Schmidt, M., Brenner, R. E., Emons, D., Dame, C., Pontz, B. *et al.* Yunis–Varon syndrome: evidence for a lysosomal storage disease. *Am. J. Med. Genet.* **95,** 157–160 (2000).
10 Dworzak, F., Mora, M., Borroni, C., Cornelio, F., Blasevich, F., Cappellini, A. *et al.* Generalized lysosomal storage in Yunis Varon syndrome. *Neuromuscul. Disord.* **5,** 423–428 (1995).
11 Rabe, H., Brune, T., Rossi, R., Steinhorst, V., Jorch, G., Horst, J. *et al.* Yunis–Varon syndrome: the first case of German origin. *Clin. Dysmorphol.* **5,** 217–222 (1996).
12 Pfeiffer, R. A., Diekmann, L. & Stock, H. J. Aplasia of the thumbs and great toes as the outstanding feature of Yunis and Varon syndrome. A new entity. A new observation. *Ann. Genet.* **31,** 241–243 (1988).
13 Chow, C. Y., Zhang, Y., Dowling, J. J., Jin, N., Adamska, M., Shiga, K. *et al.* Mutation of FIG4 causes neurodegeneration in the pale tremor mouse and patients with CMT4J. *Nature* **448,** 68–72 (2007).
14 de Leeuw, C. N. CMT4J: Charcot–Marie–Tooth disorder caused by mutations in FIG4. *Clin. Genet.* **73,** 318–319 (2008).
15 Ikonomov, O. C., Sbrissa, D., Fligger, J., Delvecchio, K. & Shisheva, A. ArPIKfyve regulates Sac3 protein abundance and turnover: disruption of the mechanism by Sac3I41T mutation causing Charcot–Marie–Tooth 4J disorder. *J. Biol. Chem.* **285,** 26760–26764 (2010).

PLOS | ONE

Performance Comparison of Bench-Top Next Generation Sequencers Using Microdroplet PCR-Based Enrichment for Targeted Sequencing in Patients with Autism Spectrum Disorder

Eriko Koshimizu[1☯], Satoko Miyatake[1☯], Nobuhiko Okamoto[2], Mitsuko Nakashima[1], Yoshinori Tsurusaki[1], Noriko Miyake[1], Hirotomo Saitsu[1], Naomichi Matsumoto[1]*

1 Department of Human Genetics, Yokohama City University Graduate School of Medicine, Yokohama, Japan, **2** Department of Medical Genetics, Osaka Medical Center and Research Institute for Maternal and Child Health, Osaka, Japan

Abstract

Next-generation sequencing (NGS) combined with enrichment of target genes enables highly efficient and low-cost sequencing of multiple genes for genetic diseases. The aim of this study was to validate the accuracy and sensitivity of our method for comprehensive mutation detection in autism spectrum disorder (ASD). We assessed the performance of the bench-top Ion Torrent PGM and Illumina MiSeq platforms as optimized solutions for mutation detection, using microdroplet PCR-based enrichment of 62 ASD associated genes. Ten patients with known mutations were sequenced using NGS to validate the sensitivity of our method. The overall read quality was better with MiSeq, largely because of the increased indel-related error associated with PGM. The sensitivity of SNV detection was similar between the two platforms, suggesting they are both suitable for SNV detection in the human genome. Next, we used these methods to analyze 28 patients with ASD, and identified 22 novel variants in genes associated with ASD, with one mutation detected by MiSeq only. Thus, our results support the combination of target gene enrichment and NGS as a valuable molecular method for investigating rare variants in ASD.

Citation: Koshimizu E, Miyatake S, Okamoto N, Nakashima M, Tsurusaki Y, et al. (2013) Performance Comparison of Bench-Top Next Generation Sequencers Using Microdroplet PCR-Based Enrichment for Targeted Sequencing in Patients with Autism Spectrum Disorder. PLoS ONE 8(9): e74167. doi:10.1371/journal.pone.0074167

Editor: Takeo Yoshikawa, Rikagaku Kenkyūsho Brain Science Institute, Japan

Received June 5, 2013; **Accepted** July 29, 2013; **Published** September 16, 2013

Funding: Research grants from the Ministry of Health, Labour and Welfare: the Japan Science and Technology Agency: and the Strategic Research Program for Brain Sciences, Grant-in-Aid for Scientific Research on Innovative Areas (Transcription cycle) from the Ministry of Education, Culture, Sports, Science and Technology of Japan, Grant-in-Aid for Scientific Research from Japan Society for the Promotion of Science, Grant-in-Aid for Young Scientist from Japan Society for the Promotion of Science, and Grant from the Takeda Science Foundation. The funders had no role in study design, data collection and analysis, decision to publish, or preparation of the manuscript.

Competing Interests: The authors have declared that no competing interests exist.

* E-mail: naomat@yokohama-cu.ac.jp

☯ These authors contributed equally to this work.

Introduction

Recent advances in next generation sequencing (NGS) technologies combined with efficient gene enrichment, allows the comprehensive resequencing of multiple known causative or associated genes in highly heterogeneous diseases. In addition, these technologies make it possible to perform resequencing more inexpensively and rapidly than the conventional Sanger method. Higher sequencing accuracy due to the deeper achievable coverage with the aid of improved bioinformatic analysis is expected as well. Different bench-top next generation DNA sequencers are currently available for target resequencing. Each NGS machine adopts specific technologies, thus the property and/or quality of sequence reads is likely different. However there is little comparative evidence on the data quality between sequencers used in human gene analysis.

Autism spectrum disorder (ASD) is a complex disorder with several hundred associated loci, following a polygenic mode of inheritance [1]. It is relatively common, with a prevalence of 1.1% [2], and is typically a child-onset disorder characterized by impaired social interactions, communication deficits, and restricted and repetitive behaviors [3]. It is known to be highly heritable, yet the majority of its heritability is so far unresolved [4]. Previous studies suggest a genetic contribution, consisting of both common and rare alleles, accounts for a portion of ASD risk, with a heritability of 38–90% [4–8]. Considering the frequency and socio-economic impact of ASD, verification of the actual heritability of ASD is of importance. Common single-nucleotide variants (SNVs) have been reported as a major source of ASD risk, with the heritability exceeding 40% [7]. However, their impact on ASD development is relatively small in each case, with an estimated odds ratio (OR) <1.2 [9]. Conversely, rare variants occurring *de novo* or inherited are assumed to affect ASD risk as well [1,10–13]. Recent work revealed a larger effect of *de novo* SNVs, although they accounted for only a small portion of overall ASD risk, with an estimated 10% contribution to ASD risk [10–13]. Recently, an additive 5% contribution to ASD risk was reported in rare complete knockouts, derived from inheriting rare